

Tropical Pacific – mid-latitude teleconnections in medieval times

**Nicholas E. Graham · Malcolm K. Hughes ·
Caspar M. Ammann · Kim M. Cobb ·
Martin P. Hoerling · Douglas J. Kennett ·
James P. Kennett · Bert Rein · Lowell Stott ·
Peter E. Wigand · Taiyi Xu**

Received: 16 February 2006 / Accepted: 18 December 2006
© Springer Science + Business Media B.V. 2007

The online version of this article (<http://dx.doi.org/10.1007/s10584-007-9239-2>) contains supplementary material, which is available to authorized users.

N. E. Graham (✉)

Hydrologic Research Center, 12780 High Bluff Drive, Suite 250, San Diego, CA 92130-2069, USA
e-mail: ngraham@hrc-lab.org

N. E. Graham
Scripps Institution of Oceanography, La Jolla, CA, USA

M. K. Hughes
University of Arizona, Tucson, AZ, USA

C. M. Ammann
National Center for Atmospheric Research, Boulder, CO, USA

K. M. Cobb
Georgia Technical Institute, Atlanta, GA, USA

M. P. Hoerling · T. Xu
NOAA Climate Diagnostics Center, Boulder, CO, USA

D. J. Kennett
University of Oregon, Eugene, OR, USA

J. P. Kennett
University of California Santa Barbara, Santa Barbara, CA, USA

B. Rein
Johannes Gutenberg-Universität Mainz, Mainz, Germany

L. Stott
University of Southern California, Los Angeles, CA, USA

P. E. Wigand
University of Nevada, Reno, NV, USA

P. E. Wigand
California State University, Bakersfield, CA, USA

Abstract Terrestrial and marine late Holocene proxy records from the western and central US suggest that climate between approximately 500 and 1350 A.D. was marked by generally arid conditions with episodes of severe centennial-scale drought, elevated incidence of wild fire, cool sea surface temperatures (SSTs) along the California coast, and dune mobilization in the western plains. This Medieval Climate Anomaly (MCA) was followed by wetter conditions and warming coastal SSTs during the transition into the “Little Ice Age” (LIA). Proxy records from the tropical Pacific Ocean show contemporaneous changes indicating cool central and eastern tropical Pacific SSTs during the MCA, with warmer than modern temperatures in the western equatorial Pacific. This pattern of mid-latitude and tropical climate conditions is consistent with the hypothesis that the dry MCA in the western US resulted (at least in part) from tropically forced changes in winter NH circulation patterns like those associated with modern La Niña episodes. We examine this hypothesis, and present other analyses showing that the imprint of MCA climate change appears in proxy records from widely distributed regions around the planet, and in many cases is consistent with a cool medieval tropical Pacific. One example, explored with numerical model results, is the suggestion of increased westerlies and warmer winter temperatures over northern Europe during medieval times. An analog technique for the combined use of proxy records and model results, Proxy Surrogate Reconstruction (PSR), is introduced.

1 Introduction

While the magnitude, scope, and character of the Medieval Climate Anomaly¹ (MCA) and to a lesser degree the Little Ice Age (LIA), are topics of considerable debate (Lamb 1965, 1977; Grove 1988; Hughes and Diaz 1994; Bradley 2000; Bradley et al. 2003a), some regional expressions of medieval climate change stand out clearly. For example, there is clear evidence for generally arid conditions across much of the western and central US from as early as 400 A.D. until about 1300 A.D., followed by a rapid shift towards a wetter regime resembling modern climate (e.g., LaMarche 1974; Stine 1994; Hughes and Graumlich 1996; Laird et al. 1996; Hughes and Funkhouser 1998; Meko et al. 2001; Cook et al. 2004). The heart of this dry western US MCA lasted from about 800–1250 A.D. and included episodes of severe centennial-scale drought, and affected regions stretching from northern Mexico, California and central Oregon, eastward through the Great Basin and into the western prairies of the central US. Proxy evidence for these changes in regional climate are documented in tree-ring series (e.g., Graumlich 1993; Hughes and Graumlich 1996; Hughes and Funkhouser 1998; Meko et al. 2001; Cook et al. 2004), sediment core palynological and salinity reconstructions (e.g., Mehringer and Wigand 1990; Davis 1992; Laird et al. 1996; Dean 1997; Byrne et al. 2001), fire-related reconstructions (e.g., Swetnam 1993; Anderson and Smith 1997; Long et al. 1998; Mohr et al. 2000), terrestrial eolian deposits (e.g., Muhs 1985; Arbogast 1996; Muhs et al. 1997; Holliday 2001; Mason et al. 2004), and lake level reconstructions (Stine 1994; Benson et al. 2002; Yuan et al. 2004; Graham and Hughes 2007).

¹Lamb (1965) introduced the term “Medieval Warm Epoch” to refer to the period of warm European summers and mild winters around 1100–1200 AD, and the designation Medieval Warm Period (MWP) has been widely used for “any climatic anomaly that occurred at some time in the historical Medieval period (500–1500 A.D.)” (Bradley et al. 2003a). Other, more widely applicable, designations have been used, for example, Medieval Climate Period (MCP) and Medieval Climate Anomaly (MCA, Stine 1994). The latter was originally used to denote the period of dry conditions in the western US and we use it here because of its general applicability.

Within the past decade, new insight into the character of Medieval climate in the western US has been afforded by a high resolution marine core reconstruction of sea surface temperature (SST) along the central California coast (Kennett and Kennett 2000). In this record, the MCA stands out clearly as a period of cool SSTs (2–3C less than modern values) from about 700–1300 A.D. (see Fig. 3), timing that closely matches the period of much reduced precipitation seen in many other proxy records from the West. This association between cool MCA coastal waters and arid conditions across the western US seen in the proxy records is reminiscent of large-scale common patterns of climatic variability over the North Pacific and North America apparent in the instrumental record and in model simulations at both interannual and multi-decadal time scales (e.g., Namias 1970; Eber 1971; Mantua et al. 1997; Cayan et al. 1998; Nigam et al. 1999; Alexander et al. 2000; Seager et al. 2005).

More recently, other evidence relevant to the scope and mechanisms of MCA climate change has become available from the tropical Pacific Ocean in the form of fossil coral and marine sediment core proxy records (Cobb et al. 2003; Stott et al. 2004; Rein et al. 2004, 2005). As noted by Cobb et al. (2003) and Rein et al. (2004), these records show that the timing of the onset and termination of the MCA dry conditions in the western US were approximately contemporaneous with transitions into and out of La Niña-like conditions in the tropical Pacific (c.f. Cook et al. 2004). While of interest on their own from climate and cultural perspectives, the changes in tropical Pacific SSTs indicated by these proxy records could explain the genesis of the MCA western droughts via familiar teleconnections between tropical Pacific SSTs and North Pacific/North American circulation patterns (Bjerknes 1966, 1969; Wallace and Gutzler 1981; Lau 1985, among many others).

This paper provides a broad review of MCA-LIA climate change as seen in a variety of proxy records from western North America and examines the hypothesis that major shifts in tropical Pacific SST patterns were an important cause of these changes. Comparisons with examples of MCA climate change from other regions are also provided, with discussion of possible links between them and the changes seen in the tropical Pacific and North America. Taken together, the results show that medieval times witnessed a distinctive pattern of climate change in many regions around the planet. As such, the findings suggest the evolution of the concept of an Atlantic-European “Medieval Warm Period” into a surprisingly sharp instance of Holocene climate change with near-global manifestations.

The paper is organized as follows: after this Introduction, Section 2 describes the data, models and statistical methods and Section 3 presents the results. Section 4 provides a summary and discussion, including comments on the relative strengths and inconsistencies of particular results, and comments on the possible connections between MCA climate shifts and cultural and environmental changes in the tropical Pacific.

2 Data and methods

2.1 Proxy data

Table 1 gives some basic information concerning the many terrestrial and marine proxy data sets used in this paper (see Fig. 1 for the locations the principal North American proxy records). More detailed information concerning many of these proxy records is given in accompanying [supplementary material Data and Methods](#). This additional information also contains a brief discussion relating to the interpretation of the California fire-related proxies (charcoal and fire scars), records we interpret (for the MCA) as primarily indicative of winter half-year precipitation deficits.

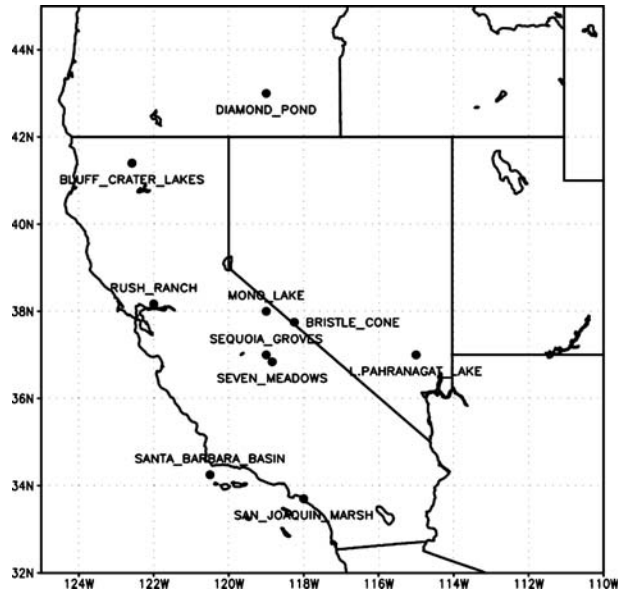
Table 1 Proxy data referred to in this study (See Supplementary Material Data and Methods and text for further discussion)

Designation	Proxy source, type (this study), climate indicator	Location	Sample resolution	Dating method, number of dates, uncertainty	Reference
Bristle Cone Pine-Nevada Climate Div. 3 precip. reconstruction, (central Nevada)	Trees, ring-width, East central California and central Nevada winter precipitation	White Mountains Eastern Calif., USA	Annual	Network chronology, annual, precise	Hughes and Graumlich 1996
Gridded PDSI	Trees, ring-width, winter precipitation	N. American	Annual	Automated network chronology, annual, precise	Cook et al. 2004
San Joaquin Marsh	Marsh core, composite flower (<i>Compositae</i>) pollen fraction, winter precipitation	Coastal S. Calif., USA	100–300 years	^{14}C , 2 last 2 kyrs, 100–200 years	Davis 1992
L. Pahramagat Lake	Lake core, conifer-saltbush pollen ratio, winter precipitation	S. Nevada, USA	~14 years	^{14}C , 24 last 5.6 kyrs, 50–100 years	Wigand 1997; Wigand and Rhode 2002
Diamond Pond	Lake core, juniper-grass pollen ratio, winter precipitation	S. E. Oregon, USA.	20–50 years	^{14}C , ~30 last 3 kyrs, 60–120 years	Wigand 1987; Mehringer and Wigand 1990
Crater Lake	Lake core, charcoal, winter precip./fuel	N. Cent. Calif, USA	~20 years	^{14}C , ~2 last 2.6 kyrs, 50–100 years	Mohr et al. 2000
Bluff Lake	Lake core, charcoal, winter precip./fuel	N. Cent. Calif, USA	35–50 years	^{14}C , ~2 last 2.7 kyrs, 50–100 years	Mohr et al. 2000
Sierra Nevada “Seven Meadows”	Terrestrial (meadow) cores, charcoal (composite from seven cores) winter precip./fuel	Sierra Nevada, Central Calif. USA	~100 years (original record not available)	^{14}C , 5–7 last 5 kyrs, 50–100 years	Anderson and Smith 1997
Giant Sequoia Groves	Redwood (Giant Sequoia) trees, fire scars from five groves. winter precip./fuel	Sierra Nevada, Central Calif. USA	Annual	Network chronology, annual, precise	Swetnam 1993

Santa Barbara Channel, Core 893A	Marine core, Foram. $\delta^{18}\text{O}$, SST	Near-coastal central Calif. USA	~25 years	^{14}C , 5 last 1.5 kyrs, 50 years	Kennett and Kennett 2000
San Francisco Bay/Rush Ranch	Marsh core, Foram. assemblage, salinity, Sacramento River flow, winter precipitation	Coastal central Calif USA	50–200 years	^{14}C , 4 last 2.6 kyrs, 50–200 years	Byrne et al. 2001; Starratt 2004
Palmyra Island	Coral $\delta^{18}\text{O}$, SST/water mass source	N. Cent. Equatorial Pacific	Sub-annual	U/Th ~50 last 1.1 kyrs	Cobb et al. 2003
Mindanao, Core MD98-2181	Marine core, Foram. Mg/Ca, SST	NW Equatorial Pacific, south of Mindanao	25–75 years	0–10 years ^{14}C , 5 last 1.5 kyrs, 100–300 years	Stott et al. 2004
Coastal Peru, Core SO147-106KL	Marine core, terrestrial sediment conc. (“lithics”), high river flow, high precipitation events.	80 km off central Peru	1–3 years	^{14}C , 8 last 2.5 kyrs, 100–300 years	Rein et al. 2004, 2005
Laguna Chichancanab	Lake core, Foram. $\delta^{18}\text{O}$, evaporation-inflow-relative drought	Yucatan Peninsula, Mexico	15–20 years	^{14}C , 4 last 3.2 kyrs	Hoddel et al. 1995
Spannagel Cave	Cave speleothem, $\delta^{18}\text{O}$, Winter temperature; westerly circulation.	Alps, Austria	2–5 years	U/Th, 9 last 2.1 kyrs, 10–60 years	Mangini et al. 2005
Chillibrillo Cave	Cave speleothem, $\delta^{18}\text{O}$, Precipitation	Panama	1–4 years	U/Th, 5 in 1.4 kyrs, 40–100 years	Lachniet et al. 2004
Bermuda	Coral, $\delta^{18}\text{O}$, SST	Bermuda	40–140 years	^{14}C , 13 in 2.8 kyrs, 30–50 years	Keigwin 1996
Uamh an Tartair Cave	Cave speleothem, $\delta^{18}\text{O}$, Precipitation	N. Scotland	annual	annual & U/Th 3	Proctor et al. 2000, 2002
Lake Naivasha	Lake core, stratigraphy, lake level, precipitation	Rift Valley, Kenya	2–35	~20 years ^{14}C 12 last 1.1 kyrs	Verschuren et al. 2000
Laguna Aculeo	Lake core, wet density, austral winter high inflow events, precipitation	West central Chile	~10 years	^{14}C 6 in 2.2 kyrs, 40–165 kyrs	Jenny et al. 2002

Winter – is winter half-year (boreal unless otherwise noted), uncertainty for ^{14}C and U/Th dating is 1 σ , uncertainties not given for tree-ring records.

Fig. 1 Locations proxy record for the western US



2.2 Climate model data

Results from both coupled ocean-atmosphere general circulation models (CGCMs) and stand-alone atmospheric general circulation models (AGCMs) are used.

2.2.1 Coupled ocean-atmosphere general circulation models

CCSM One set of CGCM results comes from an 1,150-year simulation using the National Center for Atmospheric Research (NCAR) Community Climate System Model (CCSM) version 1.4 (e.g. Boville and Gent 1998). For the simulations described here, the atmospheric component of the model was configured at triangular-31 (T31) spectral truncation giving a spatial resolution of about 3.75° with 18 layers in the vertical (top at 5 hPa). The ocean component of the model has 45 levels, 1.8° zonal resolution, and meridional resolution varying from 1.8° at higher latitudes to 0.8° near the equator. This simulation was forced with estimated changes in solar irradiance, greenhouse gas concentrations, and volcanic aerosols from 850–2000 A.D. (see Ammann et al. 2003, 2007), and the effect of this prescribed forcing is clearly apparent in the simulated surface air temperature (and SST) records from most regions. (This version of the model also shows robust centennial-scale fluctuations in sea ice concentration over portions of the high latitude North Atlantic which imprint a detectible low frequency signal on temperature in northwest Europe). The model produces more-or-less realistic El Niño variability in the tropical Pacific (Meehl and Arblaster 1998; Otto-Bliesner et al. 2003) and related extratropical teleconnection patterns. The results of this simulation show excellent agreement with N. Hemisphere warm season temperature reconstructions over the past millennium (Ammann et al. 2007), and model temperatures in most regions closely follow the changes in imposed irradiance. Despite the widespread and substantial changes in near surface temperature (land and ocean), the resulting changes in patterns of atmospheric circulation (related to the imposed irradiance variability or otherwise) are minor, and in the Pacific

sector particularly disagree with the sense of the substantial MCA-LIA changes suggested by the proxy records discussed here. For the purposes of this paper, the simulation is used as an extended control run without regard for temporal order.

ECHAM4-OPYC We also use results from 240-years of a 300-year control simulation performed with the Max Planck Institute for Meteorology (MPI) ECHAM4 (atmospheric component) – OPYC (ocean component) CGCM [see Roeckner et al. (1999) for description]. For this simulation, ECHAM4 was configured at T42 resolution (approximately 2.8° latitude–longitude resolution), with 19 vertical layers (top at 10 hPa). The ocean model has 11 vertical layers with 2.8° meridional resolution poleward of 36° latitude, decreasing to 0.5° at the equator; zonal resolution is 2.8° everywhere. The model produces a climatology that is realistic in many respects [see Roeckner et al. (1999) for details], including the depiction of El Niño variability (e.g., Timmermann et al. 1999).

2.2.2 Stand-alone atmospheric general circulation models

These results come from simulations conducted (by co-authors Hoerling and Xu) with the NCAR Community Climate Model Version 3 (CCM3, e.g., Kiehl et al. 1998) atmospheric general circulation model (this is the atmospheric component of the CCSM coupled model described above) configured at T42 resolution with 18 vertical layers (top at 10 hPa). These simulations were designed to examine the atmospheric response to the MCA changes in tropical Pacific SST suggested by the Palmyra and Mindanao (core MD98-2181) reconstructions. To provide boundary conditions for these simulations, an idealized MCA SST anomaly field was constructed to be approximately consistent with the Palmyra and Mindanao SST reconstructions and with modern patterns of interannual SST variability. As a starting point for the reconstruction, we used the first empirical orthogonal function (EOF) of December–March tropical Pacific SSTs [104°E – 60°W and 30°N – 30°S ; Smith and Reynolds (2004) data for 1950–1998]. The spatial function for this first EOF mode (the familiar “El Niño” pattern) was expressed in units of SST response and scaled over the central and eastern equatorial Pacific to give a value for the NINO3.4 index (average over 120°W – 170°W , 5°N – 5°S) of approximately -1.5°C , in agreement with difference between modern and MCA SSTs indicated by the Palmyra reconstruction. A separate weighting was applied over the western and off-equatorial central Pacific so that the maximum values in the northwest tropical Pacific were on the order of 1 – 1.5°C . To make the idealized SST changes in the western Pacific like those inferred from the Mindanao reconstruction (from core MD98-2181), a zonal extension was inserted between 178°E and 174°W to translate the SST anomalies in the western ocean farther west [this was required because observed cool (warm) SST anomalies often form in the western Pacific during El Niño (La Niña) events tend to be found well east of the Philippines]. The anomaly field was then tapered along the boundaries to reduce spatial gradients and added to modern monthly climatological SST fields. Figure 2 shows a map of the inferred SST departures from modern averages.

Two model experiments were conducted, one used the modern climatological cycle of SSTs alone (the MODERN simulation) and the other included the inferred MCA SST changes as described above (the MCA simulation). Because El Niño variability has a non-linear impact on climate (in large part because of the asymmetric response of precipitation to positive and negative SST anomalies in the eastern equatorial Pacific; e.g. Hoerling et al. 1997), an idealized El Niño–La Niña cycle was imposed in tropical Pacific SSTs in both simulations. This idealized cycle was constructed using the spatial patterns of the leading EOF of modern SSTs (calculated separately for each calendar month over 20°N – 20°S , and

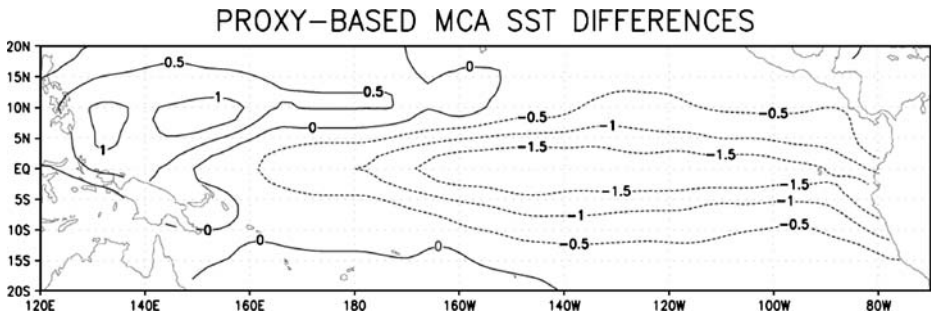


Fig. 2 Proxy-inferred tropical MCA Pacific SST pattern used for CCM3 experiments; values are differences (C) from modern averages

120E to the coast of South America for 1950–99). The EOF patterns were scaled so that the Niño3 index (area-average over the region 150–90W, and 5N–5S) varies from zero in June of Year 0 (notation of Rasmussen and Carpenter 1982), to +2°C in November–December of Year 0, to zero again in June of Year 1, reaching a minimum of –2°C in November and December of Year 2, and returning to zero in June of Year 3. To provide representative sampling, both simulations were run for 40 years so that each contains 20 El Niño and 20 La Niña episodes.

2.3 Statistical methods

Most of the techniques used here are familiar and where necessary additional details are given in the text. Windowed smoothing is applied in some cases to irregularly sampled proxy records in which averages are taken over all data points within a sliding window with a constant temporal width (e.g., 101 years), rather than over a fixed number of data points.

We introduce a new technique (Proxy-Surrogate Ranking, PSR) to assist in inferring past changes in large-scale climate and circulation. PSR is an analog method [using elements from the “trend-surface” approach described by Graumlich (1993)] in which numerical model output is reordered to obtain temporal agreement between a proxy data series (Y) and a corresponding subset of the model output (Y^* ; both Y and Y^* may be multivariate). The goal is to reorder the model output (the “surrogate” data) so that there is good serial agreement between Y and Y^* . The reordered model data can then be used to examine possible multivariate scenarios of past climate that are consistent with the original proxy data. For example, one might have a proxy-derived regional precipitation index (Y) and a corresponding index from a model simulation (Y^* ; Y and Y^* needn’t have the same length). The model index is reordered so that it agrees well (in time) with the proxy series, then this reordering applied to the full model output. The reordered model data can then be used to examine how, for example, 500 hPa heights may have evolved as consistent with behavior of the original proxy index. The PSR methodology is outlined more formally in the [Appendix](#).

In this paper, PSR is used to contrast MCA and post-MCA near-surface temperature, precipitation and large-scale circulation patterns as estimated from (proxy and model) a) central California precipitation and SST, and b) tropical Pacific SST.

3 Results

3.1 Proxy records from Western and Central US

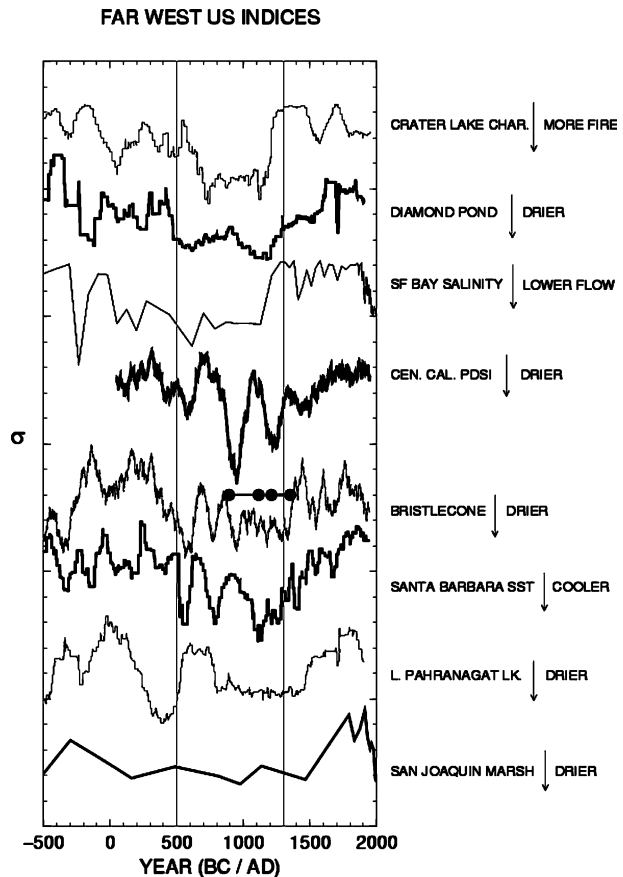
Figure 3 gives a general overview of the MCA and MCA-LIA transition in the far western US as seen in a variety of proxy records arranged loosely from north to south. Beginning in Northern California, the Crater Lake sediment charcoal record (inverted and smoothed over windows of 101 years; Mohr et al. 2000) indicates increasing fire frequency beginning in the sixth century A.D., sustained elevated frequency from the seventh through the eleventh century (values on the order of $0.75 \text{ particles cm}^{-2} \text{ yr}^{-2}$), followed by a sharp decline during the eleventh and twelfth centuries (to values $<0.1 \text{ particles cm}^{-2} \text{ yr}^{-1}$) apparently associated with changing climate at the MCA-LIA transition (increasing precipitation and/or decreasing summer temperatures). As discussed later, this general pattern of increasing fire during the MCA, then declining going into the LIA, is repeated in other fire-related proxy records from California, and is interpreted here as being caused largely by decreased in winter half-year precipitation (though warmer MCA summer temperatures may have played a role as well, see Graumlich 1993 and Millar et al. 2006).

The Diamond Pond juniper-to-grass pollen ratio record (averages of samples in 101-year blocks; Mehringer and Wigand 1990) shows a pattern of low frequency change much like that seen in the Crater Lake charcoal record, and indicates a protracted period of decreased wet season (autumn through spring) precipitation beginning from the fifth–thirteenth centuries, followed by increasing precipitation beginning approximately 1200 A.D. (coincident within dating uncertainty with the rapid decrease in Crater Lake charcoal accumulation). The juniper-grass pollen ratio changes associated with these fluctuations are quite large, going from typical values of about 0.28 from 500–1200 A.D. (the lowest sustained values during the 6,000 year record) to 1.4 during the eighteenth and nineteenth centuries. Other indices from the Diamond Pond record, including charcoal-pollen ratios and packrat midden counts, are consistent with the climate changes inferred from the juniper-grass pollen ratios (Mehringer and Wigand 1990; Wigand and Rhode 2002).

The San Francisco estuary diatom salinity index (DSI; Byrne et al. 2001; Starratt 2004) indicates increasing salinity from 2,000–1,500 years BP, relatively high salinities during the MCA, with a rapid shift towards lower salinity around 1100 A.D., implying increasing discharge from the Sacramento/San Joaquin Rivers. The timing of the inferred increase in discharge is approximately 100 years earlier than the onset of the LIA as seen in the Crater Lake and Diamond Pond records (and up to 200 years earlier than changes seen elsewhere in central California). These differences may reflect dating uncertainty and sample resolution. The shift in the DSI (fractional representation of fresh and brackish water diatom taxa as opposed to those found in saline environments) from about 25% during the MCA, to $>95\%$ during the LIA indicates salinity changes from approximately 15–20‰ to 2–7‰, respectively, suggesting that MCA Sacramento-San Joaquin discharge was as much as 40% less than twentieth century values (Byrne et al. 2001). (Note: the decline in the DSI late in the record is thought to reflect modern upstream interventions in Sacramento-San Joaquin river flow).

The inferred salinity – discharge record from the DSI described above can be compared with the tree-ring based Sacramento flow reconstruction described by (Meko et al. 2001; not shown), at least from the mid-MCA forward. The two records differ in several respects including the timing of increasing Sacramento flow at the end of the MCA (twelfth century in the DSI, fourteenth–fifteenth century in the tree-ring derived record) and in magnitude of

Fig. 3 Proxy climate records from the western US; *heavy horizontal lines with circles* indicate the Mono Lake low stands identified by Stine (1994); approximate duration of the MCA is indicated by *grey lines*; note that the Crater Lake charcoal concentration and San Francisco Bay salinity records are inverted. The San Francisco Bay salinity and San Joaquin Marsh records shown without smoothing, all other records are averages over sliding 101-year windows. Values are standard deviations (σ) for the records over the period shown; *vertical axis tick marks* are separated by 1σ



estimated MCA flow reductions (up to 40% reductions from the DSI, 10–15% from the tree-ring record).

Central California PDSI (average for grid squares centered at 37.5N/120W and 35N/120W; Cook et al. 2004) shows considerably more centennial-scale variability than Crater Lake and Diamond Pond records, but agrees approximately with those records regarding the timing of end of the MCA (about 1200 A.D.). The PDSI record suggests that the MCA was marked by three periods of relatively dry conditions during the late sixth–early seventh, ninth–tenth (this particularly severe), and late twelfth–thirteenth centuries, with intervening periods of much higher precipitation. The timing of the latter two dry periods, a common feature of the reconstructed PDSI data through much of California (with the best agreement through the central and south-central part of the state) coincides closely with the timing of two deep low stands and intervening high stand of Mono Lake documented by Stine (1994). Increasing, and less variable, PDSI values are indicated after about 1300 A.D. A reconstruction of coastal central/southern California precipitation for California Climate Division 6 (see Section 3.4.1) based on the PDSI record for southwest California (this record is very similar to the combined PDSI record shown in Fig. 3) indicates that centennial precipitation averages 75–85% of the twentieth century mean during these two Medieval droughts, with shorter periods of much more severe conditions. Graham and

Hughes (2007) obtain similar results (deficits of 19–25%) in centennial average central Sierra Nevada streamflow for those two droughts.

In terms of the general timing of the transitions into and out of the MCA, the bristlecone pine-derived central Nevada precipitation reconstructions (for Nevada Climate Division 3 – an index of area-average precipitation for central Nevada; Hughes and Graumlich 1996) show features similar to those in the records discussed above (see also the Great Basin reconstruction of Hughes and Funkhouser 1998). The onset of drying is indicated at approximately 300 A.D., slightly earlier than the changes seen in the Crater Lake and Diamond Pond records and much as seen in the central coastal California PDSI record. The transition out of the MCA is depicted at about 1350 A.D., 50–150 years later than suggested by the Crater Lake, Diamond Pond and San Francisco Bay salinity records. Note also that the difference between MCA and post-MCA reconstructed central Nevada precipitation is relatively small (about 5%) in comparison to the values obtained for California west of the Sierra Nevada.

The Santa Barbara Channel SST reconstruction (Kennett and Kennett 2000) shows clear similarity to many of the records described above. Reconstructed SST declines after about 500 A.D., reaching a minimum (approximately 11°C) during the eleventh and twelfth centuries, and then warms steadily during the nineteenth century (to approximately 13°C). The record is punctuated by high amplitude centennial fluctuations of 1–1.5°C, but uncertainties in the age model(s) make it impossible (though always tempting) to convincingly match specific features with those in other records. Nevertheless, the low frequency shifts from relatively warm pre-MCA SSTs to cooler MCA conditions, and warming during the LIA SSTs are clear and substantial both in terms of the full Holocene record (not shown; see Kennett and Kennett 2000), and in terms of modern SST variability along the central California coast [the standard deviation of annual average SST for 1950–2000 is approximately 0.7°C, slightly larger for December–March (Smith and Reynolds (2004) data)]. It is of interest to note that the bristlecone pine reconstruction of Nevada Climate Division 3 precipitation and reconstructed Santa Barbara channel SSTs have maintained a consistently positive relationship at multicentennial time scales over the last 3,000+ years.

The Lower Pahranaagat Lake conifer-to-saltbush pollen ratio record (Wigand 1997; Wigand and Rhode 2002) shows a period of quite moist conditions in the southern Great Basin at the beginning of the first millennium A.D. (pollen ratio reaching 1.75), drier conditions between about 300–500 A.D. (pollen ratios reaching 0.55), a brief period of increased moisture from 500–800 A.D., then a protracted MCA dry period ending about 1450 A.D. followed by increasing moisture availability through the nineteenth century (ratio reaching about 1.5).

The final series plotted in Fig. 3 is the San Joaquin Marsh “flower” (*Compositae*) pollen fraction record (Davis 1992). This record shows decreasing moisture availability (from 40% pollen fraction) early in the first millennium (a trend that begins much earlier, see Davis 1992), then relatively low values until the fifteenth century A.D. (pollen fractions of about 10%) when the record climbs sharply (to 60% during the eighteenth century). Box et al. (1999) document similar timing (1300–1400 A.D.) for evidence of increased flow in their analysis of a well-dated core (approximately 10 ¹⁴C dates between 0 and 1600 A.D.) from nearby Bouton Creek. This timing is in good agreement with the Pahranaagat Lake and bristlecone pine reconstructions. [Note: It is worth pointing out that the magnitude and abruptness of the inferred MCA-LIA transition is unique in the entire 6,000 year San Joaquin Marsh record (Davis 1992). At the same time, although the MCA-LIA transition is

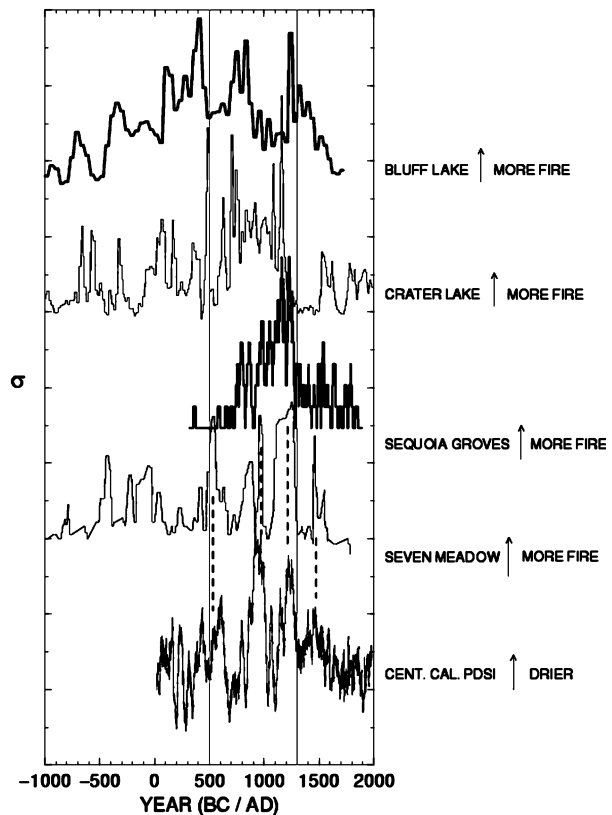
apparent in the San Joaquin Marsh vicinity, a detailed sediment core analysis from a coastal wetland 100 km to the southeast (Los Peñasquitos Lagoon near San Diego; Cole and Wahl 2000) reveals no clear signal of an MCA-LIA transition.

Considering all of the records in Fig. 3 (and recognizing that any specific age ranges will be somewhat arbitrary), there emerges a general sense that in California the MCA covered approximately 400–1300 A.D., with the most extreme conditions occurring between 800 and 1250 A.D. At the same time there is regional variability, particularly with respect to the timing of the “MCA-LIA transition” (a vague concept in any case). While many of the records suggest a transition beginning between 1100 and 1200 A.D., other records (central California PDSI, the bristlecone Nevada precipitation reconstruction, Pahrnagat Lake, and San Joaquin Marsh) suggest a rather later transition ranging from approximately 1250–1450 A.D. It seems likely that these differences reflect differential proxy responses, dating uncertainties, and varying regional climate signals (e.g., Dettinger et al. 1998) rather than important attributes of MCA climate change in the western US.

Figure 4 shows the California fire-related proxy records (described in Section 2) arranged (as in Fig. 3) more-or-less north to south. As described by Mohr et al. (2000) the records from Bluff and Crater Lakes (northern California) indicate increasing fire frequency beginning early in the first millennium B.C., peaking between 400 and 1300 A.D., then decreasing (very abruptly in the Crater Lake record) apparently in association with the increasing cool season precipitation at the onset of the LIA (other records from the region

Fig. 4 Fire-related proxy records from California; the reconstructed PDSI record for central California (*bottom; inverted*) is shown for comparison; the approximate duration of the MCA is indicated by *grey lines*. All records show averages over sliding 25-year windows. Values are standard deviations (σ) for the smoothed records over the period of record shown; *vertical axis tick marks* are separated by 1σ . *Dotted lines* emphasize alignment of maxima in the Seven Meadows charcoal record and dry periods in the PDSI record

CALIFORNIA FIRE-RELATED PROXY RECORDS



show similar behavior, see Daniels et al. 2005). The Sequoia Groves fire-scar record [Swetnam 1993; processed here to give a binary record (one if three or more groves had fire, zero otherwise) then smoothed with a 25-year running mean], shows timing similar to the Crater Lake record, with fire activity increasing in stages—first in the eighth century, again in the early tenth century, and once more in the twelfth century (during the two peaks at this time, the “four or more groves with fire” index was exceeded in more than 30% of the years) – then decreasing abruptly beginning early in the thirteenth century. The composite Seven Meadows charcoal deposition rate record (Anderson and Smith 1997) shows high amplitude variability at time scales from decades to centuries with an overall envelope similar to the Crater Lake and Sequoia records. Charcoal concentrations peak four times after about 500 A.D. in general synchrony with the tendencies in the Sequoia Groves record and fall rapidly during the thirteenth century. The agreement between the major charcoal peaks in the Seven Meadows record and the driest periods in the reconstructed PDSI record for the grid square covering the central Sierra Nevada (shown inverted in Fig. 4) emphasizes the role of precipitation deficits in contributing to the timing of periods of increased MCA fire incidence this region.

3.2 Analyses of gridded PDSI data

In this section, the Cook et al. (2004) gridded PDSI reconstruction is used to more fully examine the spatial-temporal structure of MCA-LIA precipitation changes over the western US, here using EOF analysis rather than the “drought area index” approach employed by Cook et al. (2004). The EOF analyses were performed using the 900–1992 “no missing” dataset (Section 2). A 15-year running average applied prior to analysis to emphasize lower frequency variability. Figure 5a shows the spatial pattern for the first EOF mode from a covariance matrix-based analysis in terms of correlations between the (15-year running mean) grid point time series and the temporal function (50% of the total variance of the smoothed data). The spatial signature for this mode reflects the broad spatial coherence of low frequency precipitation variability across the western US, as reported earlier by Hughes and Funkhouser (1998), with correlations exceeding 0.8 (indicating dry MCA, and moist LIA, conditions) reaching across the Great Basin to the Rocky Mountains, and from Wyoming to Arizona and New Mexico. The time function for this EOF (Fig. 5c) shows a shift towards more moist conditions with markedly fewer extended dry periods after the late thirteenth century, with suggestions of especially dry periods during the tenth, twelfth, and early-to-mid thirteenth centuries, timing that corresponds approximately with the low stands of western Great Basin lakes (Mono, Pyramid, Walker) noted by Stine (1990, 1994), Benson et al. (2002), and Yuan et al. (2004). Also shown in Fig. 5c is the (15-year running averages) Palmyra coral-based NINO3.4 SST reconstruction (Cobb et al. 2003). Beyond the general timing of the increasing precipitation through the last millennium, there are indications of agreement on shorter timescales for the segments covering the twelfth and fourteenth centuries, but such agreement is not obvious for the other segments.

To focus more closely on signal coherence rather than signal amplitude, a correlation matrix-based EOF analysis (Fig. 5b) was also conducted using the 15-year smoothed “no miss” PDSI dataset as described above. In these results, the MCA-LIA signal is captured in the second EOF mode [21% of the standardized variance; the first mode (not shown) is dominated completely by multi-decadal variability in southern British Columbia]. For the second correlation EOF mode, the maximum positive correlations (dry MCA) are found over Nevada and in comparison with the covariance matrix results the higher correlations are shifted west and northwest, reflecting coherent but lower amplitude PDSI variability

Fig. 5 **a** Loading patterns (expressed as correlations with temporal amplitudes) for first covariance mode EOF calculated from the gridded reconstructed PDSI data for all points with no missing data from 900–1989 A.D. The data were filtered with a 15-year moving average prior to the EOF analysis. This mode accounts for 50% of the total variance; correlations between the gridded time series and the temporal amplitude are shown. **b** As in panel a, but for the second EOF mode calculated using the correlation matrix (21% of the total standardized variance). *Gray shading* in each panel indicates spatial domain of EOF analysis. **c** Temporal amplitudes from the first covariance mode EOF (*light*; see panel a). The Palmyra coral NINO3.4 SST reconstruction (*dark*; arbitrarily scaled) is shown for comparison

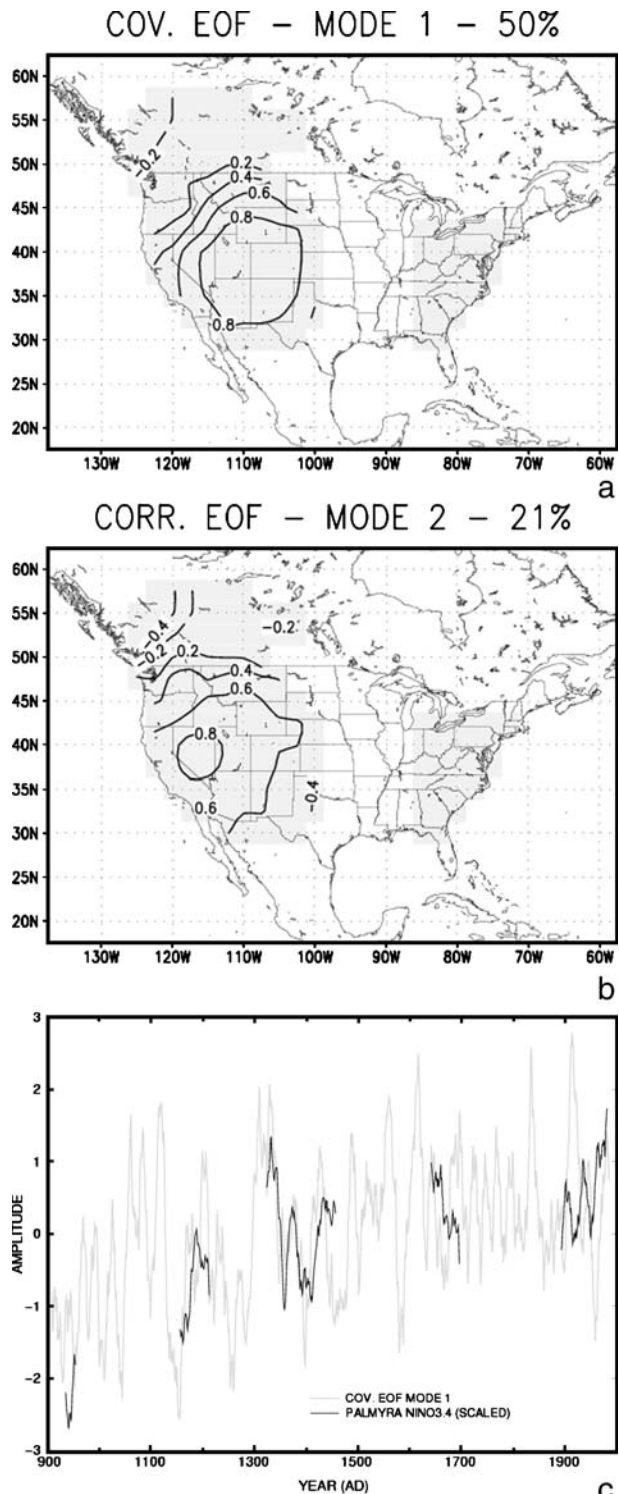
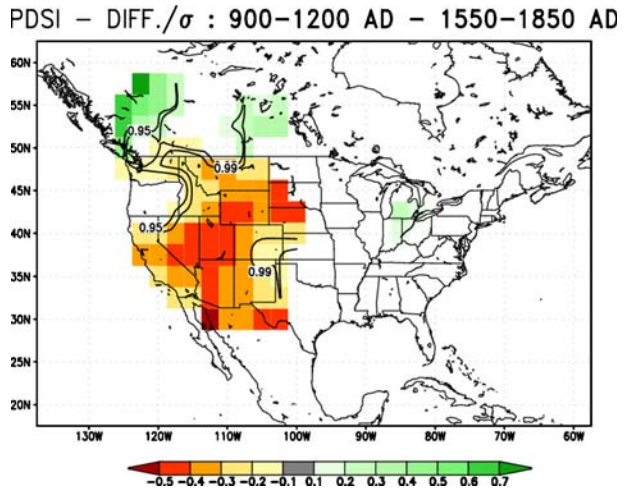


Fig. 6 Differences in reconstructed PDSI means for 900–1200 A.D.–1500–1850 A.D.; values are scaled by the standard deviation of the (*unsmoothed*) data for each gridpoint over 600-year comparison period and are shown only where *t*-test confidence levels for the difference in the means exceed the 90%; contours show the 95 and 99% *t*-test confidence levels



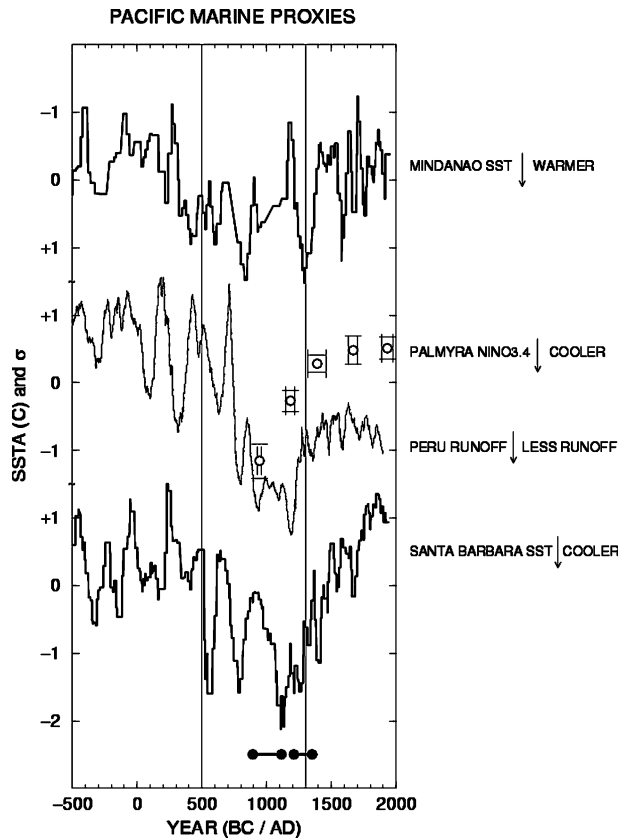
over California and western Nevada, consistent with the results of Hughes and Funkhouser (1998). Another difference between the covariance and correlation EOF results is the amplification of the negative correlations (up to 0.4) over western British Columbia in the latter. While PDSI variability in this region may relate more closely to late spring and early summer (rather than winter) conditions, the dipole-like correlation pattern second correlation EOF (Fig. 5b) is suggestive of well-known patterns of precipitation change associated with interannual to inter-decadal Pacific climate variability (e.g., Cayan et al. 1998). The temporal function for this second correlation-based EOF mode is nearly identical to that for the first covariance mode in Fig. 5c.

To get a clearer idea of the patterns and magnitudes of MCA vs. LIA changes in PDSI (and some idea of the patterns of change in precipitation), Fig. 6 shows differences between the reconstructed PDSI averages (non-smoothed data from the “no missing” dataset) for 900–1200 A.D. less that for 1550–1850 A.D. scaled by the overall standard deviation for those 600 years. By this measure, the largest negative changes (-0.4 to -0.5σ) are distributed in a pattern similar to that seen in the correlation-based EOF (Fig. 5b), with the largest negative values (drier MCA) extending from southern Wyoming and western Nebraska south through the Great Basin and extending west into central California. Large increases in reconstructed PDSI (0.5 – 0.7σ ; more moist MCA) appear in British Columbia [the area-average record for this region (not shown) shows sharply decreasing PDSI between 900 and 1200 A.D.], again indicative of the tendency for meridional polarity in MCA-LIA winter-spring climate changes over the western North America, likely the signature of shifts in large-scale circulation patterns. [The statistical significance of the grid point differences in the MCA-LIA means were estimated with a *t*-test (see Fig. 6). The significance levels obtained are little affected for reasonable choices of the number of degrees of freedom – a value of 200° was used here, allowing for the typical decorrelation time for the gridded PDSI data of 2 years].

3.3 MCA-LIA changes in the tropical Pacific

Figure 7 shows the three tropical Pacific marine proxy records described in Section 2 [(Palmyra coral, coastal Peru (core SO147-106KL) and Mindanao (core MD98-2181)], along with the Santa Barbara Channel SST reconstruction (repeated from Fig. 3). The

Fig. 7 Pacific Ocean marine proxy records; values (as anomalies) are °C for the Mindanao, Palmyra (NINO3.4) and Santa Barbara SST reconstructions and standard deviations (of the smoothed data) for the Peru river discharge reconstruction. The Mindanao, Santa Barbara and Peru records are averages over sliding 51, 101, and 51-year windows, respectively. The Palmyra data are anomalies with respect to the full reconstructed NINO3.4 SST record, plot shows segment means (*circles*), 95% confidence limits (*horizontal lines*) and segment time span (*vertical bars*). *Heavy horizontal lines with filled circles (bottom)* indicate nominal periods for the Mono Lake low stands (from Stine 1994)



Mindanao SST reconstruction (Stott et al. 2004) shows SSTs in the northwestern equatorial Pacific increasing (downward in the inverted record shown in Fig. 7) in stages beginning about 300 A.D., reaching 1C above the modern regional annual average (i.e., about 28.5 C) during the fifth century A.D., and 29C during the eight–ninth centuries and again in the thirteenth–fourteenth centuries. After the thirteenth–fourteenth centuries SSTs decline to near modern (reconstructed) values by the fifteenth century. The MCA increases in SST are substantial, representing 1.4–2.0 times the modern standard deviation of annual average SST of about 0.7C. Also note that modern SST variability in this region shows little association with either El Niño or Pacific decadal variability, both of which have their major northwestern tropical Pacific expression farther east (these generally vary in opposition to those in the central and eastern tropical Pacific).

In contrast to the much warmer (than modern) MCA SSTs indicated in the Mindanao (core MD98-2181) western Pacific reconstruction, the Palmyra NINO3.4 reconstruction (Cobb et al. 2003) suggests that MCA SSTs in the central equatorial Pacific SSTs were much cooler than (as much as -2°C) than in the modern climate, then warmed rapidly through the fifteenth century. The segment averages (Fig. 7) mask the considerable higher frequency variability apparent in the complete records [see Cobb et al. (2003) for complete discussion; 15-year smoothed records are shown in Fig. 5c], and the long inter-segment gaps further challenge interpretation. Nevertheless, the SST changes between the first three segments are much larger than the 2σ bounds on the segment means, and the reconstructed

MCA SSTs averages are more than two (interannual) standard deviations below modern annual averages. As discussed by Cobb et al. (2003), the magnitude of the reconstructed Palmyra SST fluctuations may be somewhat exaggerated by the effects of sea water $\delta^{18}\text{O}$ changes associated fluctuations in precipitation and changes in upwelling and horizontal advection (“salinity” effects) – and more refined thermometry measurements [e.g. Mg/Ca (Mitsuguchi et al. 1996)] may eventually resolve this issue. In any case, Woodroffe and Gagan (2000) and Woodroffe et al. (2003) considered this issue in some detail in their Holocene SST reconstructions from nearby Christmas Island and determined that the impact of water mass isotopic variability (the “salinity” effect) on $\delta^{18}\text{O}$ SST reconstruction was modest.

The opposing trends in reconstructed SST in the core MD98-2181 (Mindanao) and Palmyra records over the past millennium suggest the intriguing scenario of an MCA marked not only of a relatively cooler eastern and central tropical Pacific, but also by substantial warming in the western equatorial ocean (i.e., a substantial increase in the equatorial Pacific zonal SST gradient). Further, the Mindanao record raises the suggestion that the Palmyra record portrays just the latter half of the MCA episode, i.e. a preceding cooling phase is not covered. Support for this scenario comes from the riverine sediment concentration record from Core SO147-106KL from near-coastal central Peru (Rein et al. 2004, 2005). This record shows increasingly large excursions towards low concentrations of riverine deposits [indicative of reduced flood frequencies in coastal northern Peru and Ecuador] beginning during the early first millennium A.D., approximately coincident with the onset of warming in the Mindanao SST reconstruction. The record is marked by a particularly large decrease during the eighth century AD, with further declines leading to minimum values during the tenth–twelfth centuries. A rapid recovery towards higher terrestrial material concentrations begins early in the thirteenth century [in close synchrony with the precipitation and fire related changes in California (Figs. 2 and 3)].

The Santa Barbara Channel SST reconstruction (repeated from Fig. 3) is also shown in Fig. 7. The remarkable similarity between this record and those from the tropical Pacific (a 2°C decrease in SST between 300 and 1100 A.D., with superimposed energetic centennial fluctuations; rising SSTs after the twelfth century) is clear and consistent with (tropical-mid-latitude) associations apparent in both the instrumental record and model results, and well understood on the basis of physical processes.

3.4 Syntheses

3.4.1 Cross-proxy reconstruction vs. cross-instrumental record relationships

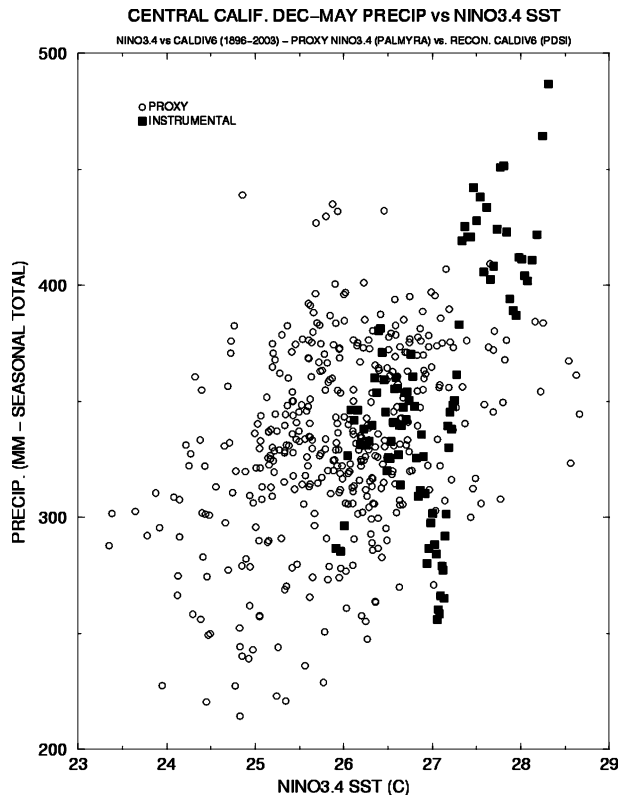
While the qualitative consistency between the associations noted among proxy reconstructions and those found in observations and model results is suggestive of the character of climate change, quantitative consistency allows increased confidence in the precision of the proxy records. In this section, two such cross-proxy comparison analyses are presented relating to the association between tropical Pacific SSTs (Palmyra reconstruction) and California climate.

The positive association between precipitation in much of the western US and tropical Pacific SSTs as seen in the instrumental record is well known (e.g., Ropelewski and Halpert 1987; Schonher and Nicholson 1989; Redmond and Koch 1991), and qualitatively supports the idea of a connection between the cool eastern tropical Pacific SSTs (Figs. 5c, and 7) and generally dry conditions across the western US (Figs. 3, 4, 5, and 6) during the MCA. Beyond qualitative support, the question arises whether the proxy-inferred precipitation

changes over the western US are of the magnitude that would be expected given the proxy-inferred changes in tropical Pacific SSTs?

Addressing this question requires first an estimate of the magnitude of MCA reductions in western US precipitation. As a starting point for such an analysis, a statistical model was constructed relating reconstructed PDSI (average for the two grid points centered at 35N 120W and 35N 117.5W) to observed precipitation over coastal central and Southern California (California Climate Division 6; November–May totals for 1895–96 to 1997–98). The resulting exponential model gives a good fit ($R=0.83^*$) in which divisional precipitation showing an increasingly positive response as reconstructed PDSI increases. This relationship was then used to produce a reconstruction of regional precipitation from the reconstructed PDSI data. The relationship between these data and Palmyra-inferred NINO3.4 SST is shown in Fig. 8 (for this figure the reconstructed precipitation and SST records were smoothed with a 15-year running mean to allow for dating uncertainty in the latter). The resulting scatter plot shows an approximately linear relationship giving an increase of about 100 mm of seasonal total precipitation over the 24–28°C range covered by the proxy SST record. Figure 8 also shows the distribution between historical NINO3.4 SST (Kaplan et al. 1998 data) and California Division 6 precipitation. This distribution shows a positive association (as expected) but the slope is steeper than that in the proxy reconstructions. (Note: the dip in the observed distribution near 27°C results primarily from a relatively small number of particularly dry years that occurred when SSTs were not especially cool; these include 1943, 1945, 1947, 1961, 1964, 1990, 2002). Recognizing the

Fig. 8 Coastal southern California (California Climate Division 6) December–May precipitation plotted as a function of NINO3.4 SST. *Open circles* show proxy reconstructed precipitation (see text) vs. the Palmyra coral NINO3.4 SST reconstruction. *Filled squares* show the same relationship for observed California Division 6 precipitation vs. NINO3.4 [Kaplan et al. (1998) data]. Proxy data are from 15-year running means; instrumental data are 15-sample averages from seasonal means sorted on the basis of NINO3.4 SST



substantial uncertainties underlying the proxy-based reconstructions, and the fact that historical NINO3.4 data is somewhat uncertain in the early years, the results in Fig. 8 may be summarized as (at least) consistent with the hypothesis that the two distributions reflect the same underlying processes.

Another “cross-proxy” relationship that can be tested quantitatively is that between tropical Pacific and central California coastal SSTs. This relationship is strong in the instrumental record, as emphasized by the mapped correlations (Fig. 9) between December–March-average Pacific Basin SSTs and NINO3 SST [Smith and Reynolds (2004) data; broadly similar patterns are found at multi-decadal time scales, e.g., Cayan et al. 1998; Mantua et al. 1997]. Of particular note in Fig. 9 are the correlations between SSTs in the tropical Pacific and those along the coast of California, which emphasize the strong positive association between SSTs in these regions. To investigate whether this relationship is similar in the proxy reconstructions and observed data, Fig. 10 shows December–March south-central California coastal SSTs [data from Smith and Reynolds (2004); 2° grid square centered at 34N 120W 1853–54 to 2001–02] with those from the NINO3.4 region (5N–5S, 170W–120W) for the instrumental record, and for those inferred from the Santa Barbara Channel and Palmyra NINO3.4 SST reconstructions. When plotted as annual averages, the observational data show an approximately linear relationship in which a 1.0°C increase in NINO3.4 SST is associated with a 0.70°C increase in coastal California SST (0.67°C coastal per 1.0°C NINO3.4 for 15-year averages). The proxy data show reasonably good agreement with these values, with slopes of 0.45 and 0.62°C coastal per 1.0° NINO3.4 for averages calculated over the Palmyra segment intervals or Santa Barbara Channel reconstruction sample intervals, respectively. [Note that when the observational data are plotted as (paired) 15-year running means, the approximately linear relationship is apparent only in the data after about 1950 (see Fig. 10 in which this period is seen in the upper right limb of the smoothed data). Whether this departure from a more or less monotonic relationship for longer term averaging is an artifact or represents the actual behavior has not been investigated.]

As mentioned in the Introduction, the evidence from proxy records for cool SSTs off coastal California and in the central and eastern tropical Pacific, along with arid conditions in the western US during the MCA, has obvious similarities to patterns seen in the modern climate record in association with El Niño/La Niña (ENSO) and Pacific inter-decadal variability. At the same time, it is worth keeping in mind that there are (at least) two clear differences between the “canonical” patterns constructed from the modern record and what

Fig. 9 Correlations between December–March NINO3.4 SST and SST elsewhere [Smith and Reynolds (2004) data, analysis period 1950–2003]; regions where correlations are above 0.6 are shaded

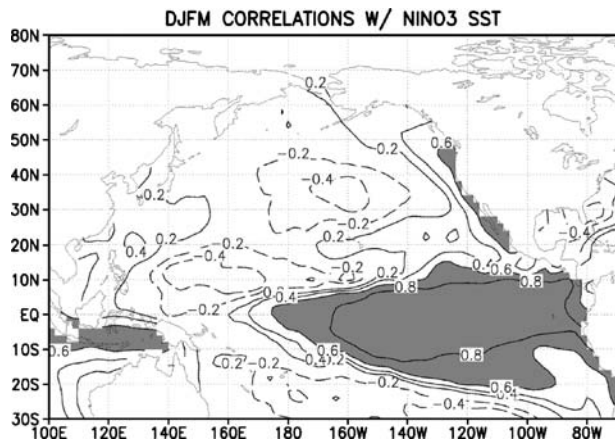
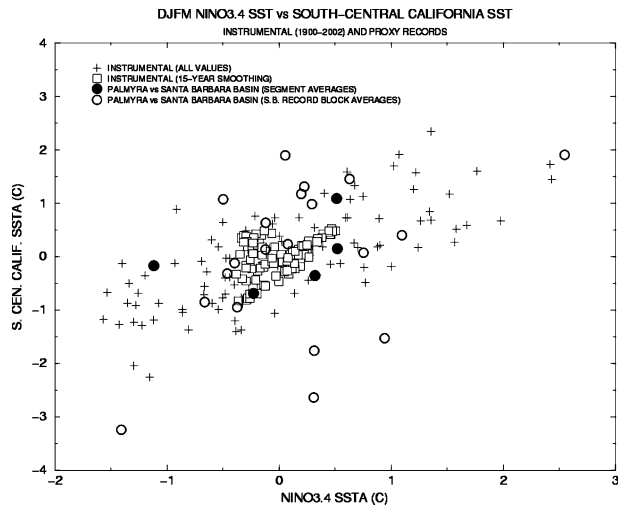


Fig. 10 South-central coastal California SST plotted as a function of NINO3.4 SST. *Circles* show proxy data (from Santa Barbara Basin and Palmyra coral reconstructions) averaged over the five sections of the Palmyra coral record. *Crosses* show the values from the instrumental record [Smith and Reynolds (2004) data; analysis period 1900–2002]; California coastal SSTs from grid point at 34N/119W



the MCA proxy data show for the western US. First, the MCA arid conditions evidently covered nearly all the western US, changing sign near the Canadian-US border (Fig. 6). In contrast, modern precipitation patterns associated with ENSO and Pacific inter-decadal variability generally show a change in sign running west-to-east across the south-central part of the western US (e.g. Mantua et al. 1997), nearly 1,000 km to the south of its position in Fig. 6. This point of dissimilarity indicates that the circulation changes that characterize the MCA were (at least for protracted times) different than those seen in typical modern composites, perhaps with cool season eastern North Pacific westerlies withdrawing north of the extreme locations seen in the instrumental era (see discussions in Rajagopalan et al. 2000 concerning modern variability in composite patterns). Second, the MCA droughts in the western US far exceed those in the modern record (and over the past 500 years or more) in terms of persistence. This persistence argues for long-lived changes in the surface forcing fields that determine favored longwave configurations in the westerlies. These two points of dissimilarity emphasize that while circulation analogues from modern times are likely of value for guidance, their quantitative applicability may be limited.

3.4.2 Inferences from model data

Composites based on California temperature and SST Numerical model results offer an opportunity to extrapolate the proxy-inferred changes in precipitation and SSTs described above. As a first means of doing so, we apply the PSR methodology (see Section 2.3 and Appendix) to results from the NCAR and MPI coupled models (see Section 2 for discussions of models and methodology). In the first set of PSR analyses, the proxy data vector (\mathbf{Y}) is given by values of the Santa Barbara Channel SST reconstruction (linearly interpolated to annual values for this analysis) and the reconstructed precipitation record for California Climate Division 6 described above. The corresponding surrogate data vectors (\mathbf{Y}^*) are composed of A) area-averaged SST from the region 33–35N, 130–123W, and B) area-averaged precipitation over the region 34–37N and 118–120W (both December–March averages), taken from the CCSM and MPI coupled models. The measure of similarity (S) is simply the Euclidean distance between the \mathbf{Y} and \mathbf{Y}^* , with coordinates of each expressed in terms of fraction of climatology (precipitation) and °C (SST).

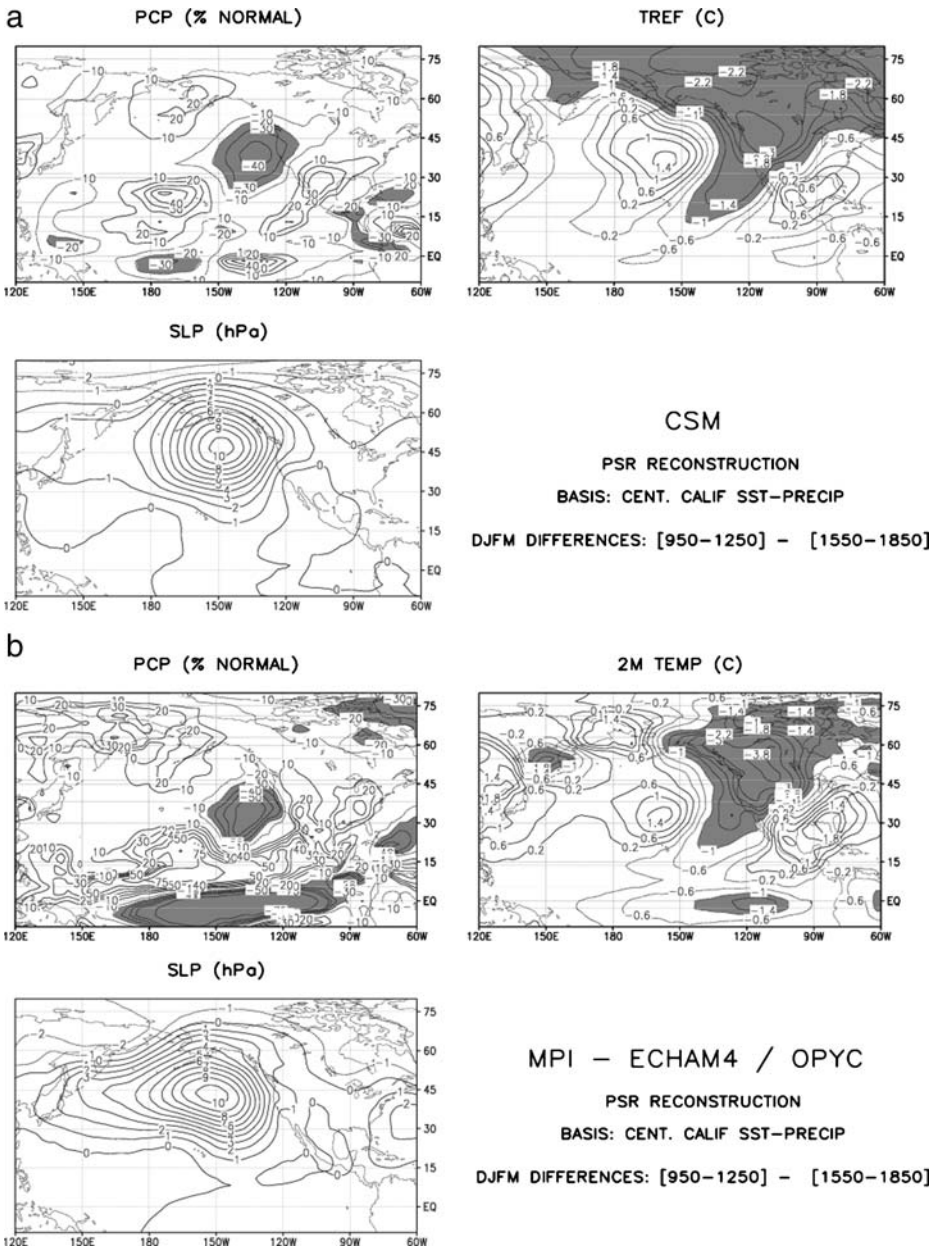


Fig. 11 a Differences between CCSM model PSR composites conditioned on proxy California coastal SST and precipitation for 950–1250 A.D. and 1550–1850 A.D. for SLP (hPa, *bottom left*), precipitation (difference as a percent of the average for the 600 years; *top left*), and surface air temperature (C, *top right*). Contour intervals are 2 hPa, 10% and 0.4C, respectively. **b** As in panel a, but from the MPI model

Figure 11a shows MCA-LIA differences between PSR-derived December–March averages in CCSM sea level pressure (SLP), precipitation, and surface air temperature (averages for 950–1250 A.D. less those for 1550–1850 A.D.). The SLP pattern show strong ridging over the North Pacific, with positive anomalies of up to 10 hPa over the Northeast

Pacific ($>1\sigma$ over much of the northeast Pacific) indicative of a weakened Aleutian Low. The precipitation composite difference shows decreases of 10% over a large parts of the western US and Canada, and 20–30% over central and Northern California and southern Oregon. The surface air temperature difference map suggests that the dry MCA winters were cool (2–3°C cooler than the LIA) across the western US and Canada. The pattern of temperature differences over the North Pacific shows negative anomalies in the east (as constrained by the compositing process) and positive anomalies in the central ocean, as would be expected with the accompanying SLP pattern.

An identical analysis applied to the MPI ECHAM4 / OPYC coupled model output (Fig. 11b), produces magnitudes and patterns of change over the northeast Pacific and western North America that are similar those obtained from the CCSM (Fig. 11a). A notable difference is that negative precipitation anomalies in the MPI pattern extend only into the western parts of California and Oregon rather than well into the interior western and west-central US as indicated in the CCSM results and as seen in reconstructed precipitation for the Great Basin (Hughes and Funkhouser 1998) and the PDSI composites (Fig. 6; Cook et al. 2004). The MPI and CCSM results also differ considerably in the tropics and subtropics with former showing a La Niña-like SST pattern and much reduced precipitation over the near-equatorial central and eastern Pacific, with extensive areas of associated above normal precipitation in the Pacific sub-tropics and over the western tropical Pacific.

When considering Fig. 11a and b, it is worthwhile to recall that these PCR composites are based (in part) on central California precipitation. This choice of indices tends to isolate both the spatial coverage of the region of MCA aridity in the western US to southern Oregon and California (unlike the patterns in Figs. 5a, b and 6), and limits the eastward extent of the north Pacific positive SLP differences into the interior western US. By construction, a composite based on regional precipitation (or “drought index”) over the western US and SST would produce MCA precipitation deficits over the west and it would likely show the North Pacific region of SLP differences extending somewhat farther to the east.

Composites based on MCA-LIA differences based on Palmyra SST Figure 12a–b show the PSR-derived MCA-LIA composite differences for CCSM and MPI coupled models constructed on the basis of the Palmyra coral NINO3.4 SST. The time periods used for comparison correspond to segments 1 and 2 of the Palmyra record (MCA; 928–961 A.D. and 1149–1220 A.D.), and segments 3 and 4 (LIA; 1317–1463 A.D. and 1635–1703 A.D.) (see Fig. 5c). For these composites, the similarity measure was the (absolute) difference between the Palmyra and model simulated NINO3.4 anomalies (calculated from the full records for all data sets). [Note: because the range of the Palmyra coral-based NINO3.4 reconstruction is larger than that in the coupled model (MPI especially) results, the same model years are selected during a few short periods of time and have been retained in the PSR reconstructed data sets).

The NINO3-based MCA-LIA differences for CCSM (Fig. 12a) show an SLP pattern similar to those derived on the basis of the California proxy data (Fig. 11a, b), though the maximum SLP differences over the North Pacific are smaller (6 hPa as opposed to 10 hPa) and the ridging over the eastern North Pacific extends slightly farther east in the Palmyra composite. Similarly, the precipitation differences are smaller in magnitude to those seen in Fig. 11a, though reductions of more than 10% cover much of the far western US, with 20–30% reductions over much of California. A difference between the North American and tropical Pacific-based precipitation-based MCA-LIA differences is that the region of reduced precipitation over the eastern North Pacific and California is moved slightly

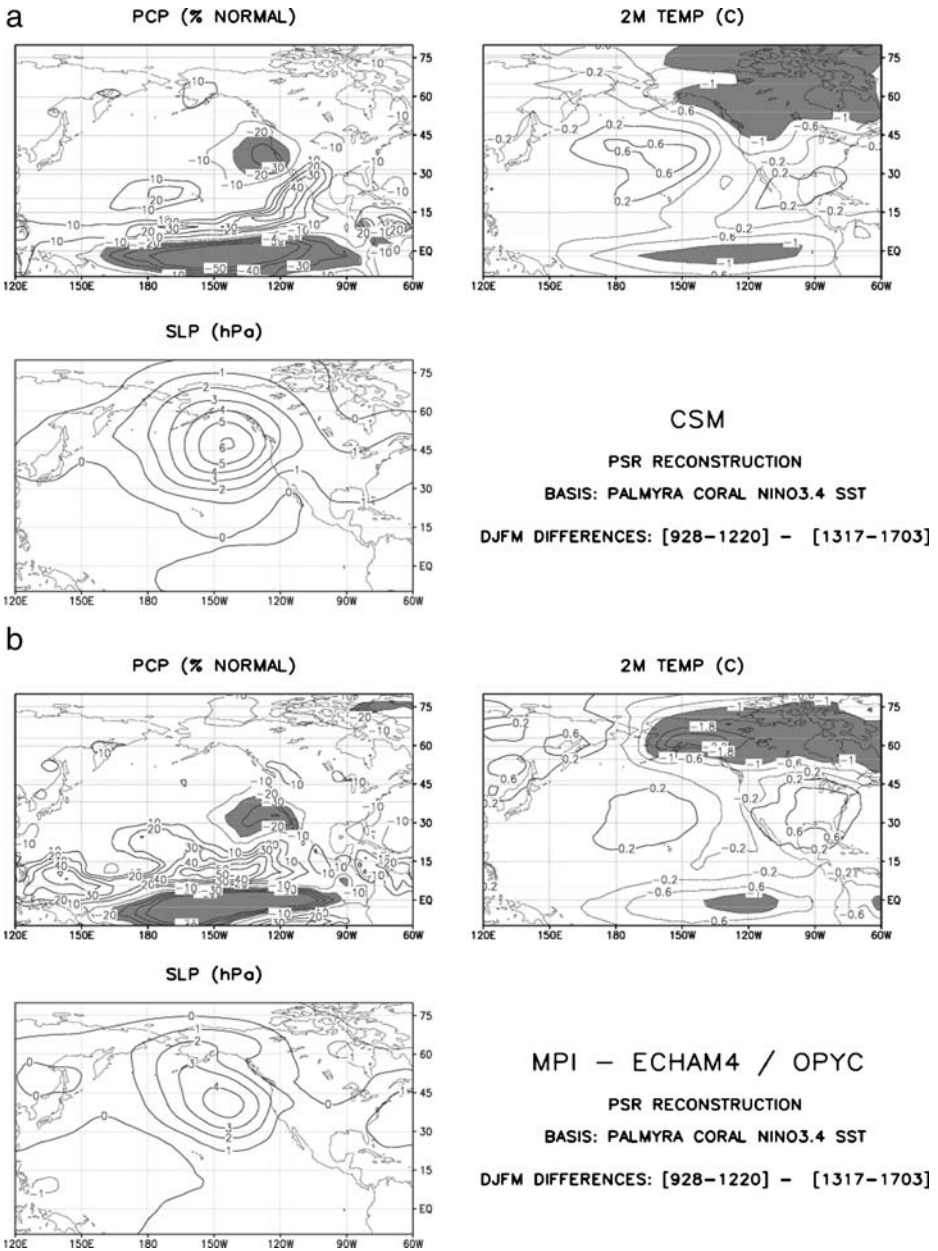


Fig. 12 **a** As in Fig. 11a, but for CCSM model PSR composites conditioned on Palmyra coral reconstruction of NINO3.4 SST; differences are for portions of the period 928–1220 and 1317–1703 for which there are reconstructed data. **b** As in panel a, but from the MPI model

southeastward in the latter. The results show increased precipitation across northern Mexico and south-central US (a spurious response of CCSM to El Niño variability), in this case extending southwestward into the off-equatorial tropical Pacific to connect with an enhanced ITCZ (precipitation increases on the order of 30%, while rainfall over the central

equatorial Pacific shows MCA reductions up to 50%. The CCM Palmyra-based MCA-LIA surface air temperature difference pattern is similar in character to that based on the California proxy records (Fig. 11a), though again the extra-tropical values are generally smaller (particularly in the eastern North Pacific), and (by construction) the cool tropical Pacific stands out clearly.

Comments similar to those above apply to the comparison between the MPI model Palmyra-based (Fig. 12b) and California proxy-based MCA-LIA composite differences (Fig. 11b). Again, the extra-tropical responses are similar in pattern but are smaller in magnitude in the former, the precipitation changes over the western US are positioned farther south. The patterns over the tropical Pacific are similar in either set of difference maps (as expected with the similar SST fields).

Results from prescribed proxy-inferred SST experiments Figure 13a shows MCA-modern differences from the CCM3 proxy-derived SST experiments (see Section 2.2.2) for November–March. The 500 hPa (500 hPa fields are shown as SLP data were not archived) differences show a pattern much like that seen in the PSR composite difference maps (Figs. 11 and 12), though the largest changes over the North Pacific (40 m) are quite modest, and suggest SLP differences of about 4 hPa [using a rough correspondence of 10:1 for 500 hPa height anomalies (in meters) to SLP anomalies (in hPa)]. The precipitation map shows a pattern similar to the PSR reconstructions, though the magnitude is only about 10% of the modern mean. The surface air temperature differences are also relatively small (-1°C maximum) in comparison to those in the PSR composites and limited in extent to southwest Canada and the northwest US.

The CCM3 simulation difference maps for March–June (Fig. 13b) from the prescribed SST simulations portray more extreme climate changes over North America. The 500 hPa field shows a zonally elongated pattern with larger negative anomalies over Canada (in comparison to the November–March result). The resulting enhanced westerly components result in a belt of decreases in precipitation of 15–20% across much of the central and south-east US. This pattern is much like that obtained by Herweijer et al. (2006; cf. Seager et al. 2005) for decadal mean PDSI anomalies in their AGCM simulations of two MCA North American droughts (these simulations also use tropical Pacific SSTs developed from the Palmyra record as prescribed forcing), and similar patterns appear in PSR coupled model SLP composites for March–June (analogous to those in Figs. 11 and 12, not shown). A recent analysis of the morphology of modern sand dunes and those that were active during the MCA in the Nebraska Sand Hills (central US) provides observational evidence for such a shift towards more westerly wind components during the MCA (Sridhar et al. 2006). Their work shows while the modern wind regime produces west-southwest to east northeast transverse dunes, the fossil MCA dunes are longitudinal, oriented in a west-northwest to east-southeast direction. Simulations show this MCA orientation requires a westerly shift (from southerly towards southwesterly) in the prevailing winds during spring and summer, a change qualitatively consistent with the “cool tropical Pacific forcing” model results discussed above.

3.4.3 The MCA signal in other regions

While the character of medieval climate has been described and debated for nearly half a century, it seems useful at this point to consider records from outside the regions focused on above as they may relate to the changes described above, in particular to the suggestion of a substantial MCA excursion in tropical Pacific SSTs. A recent record that shows

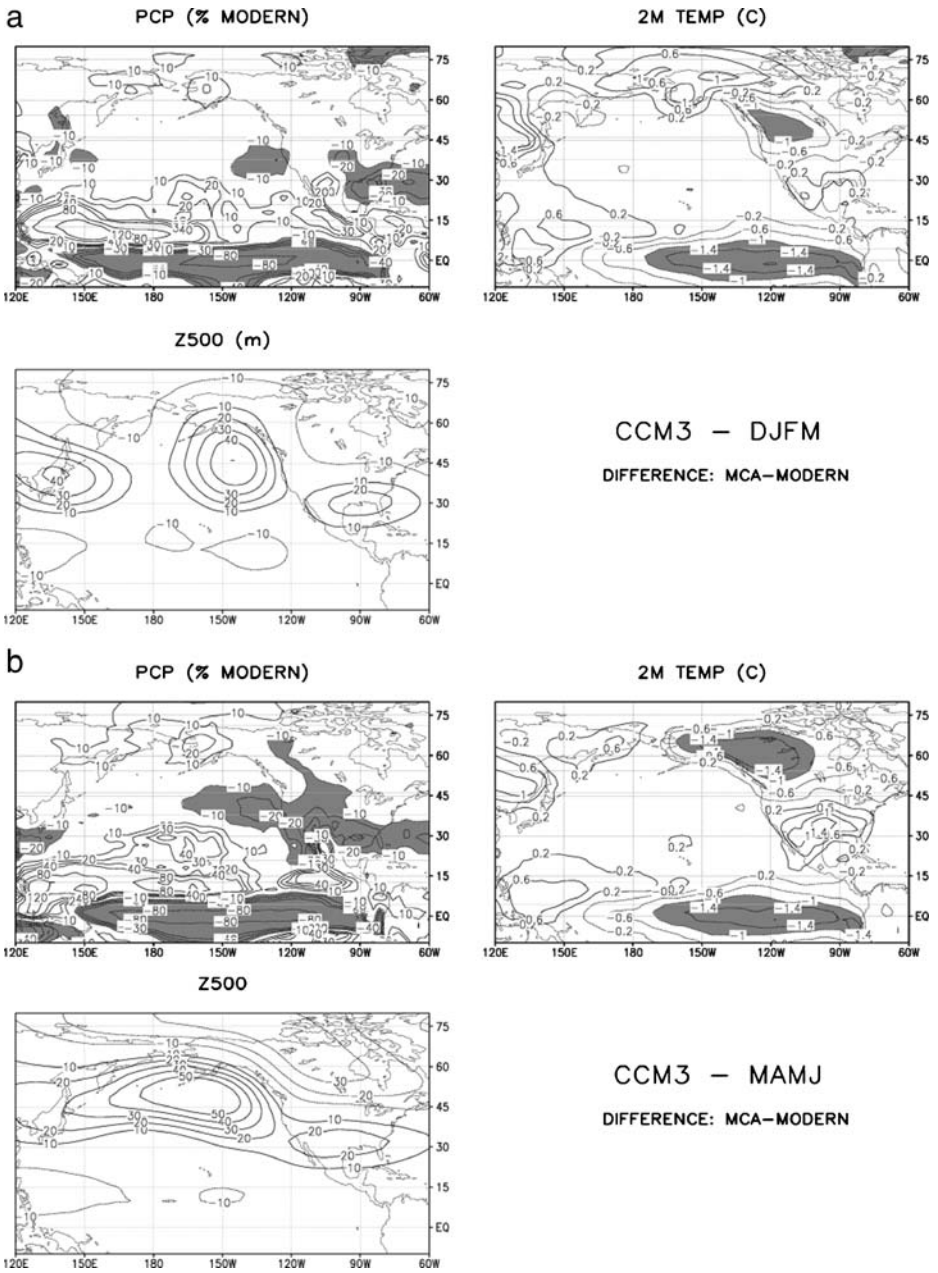
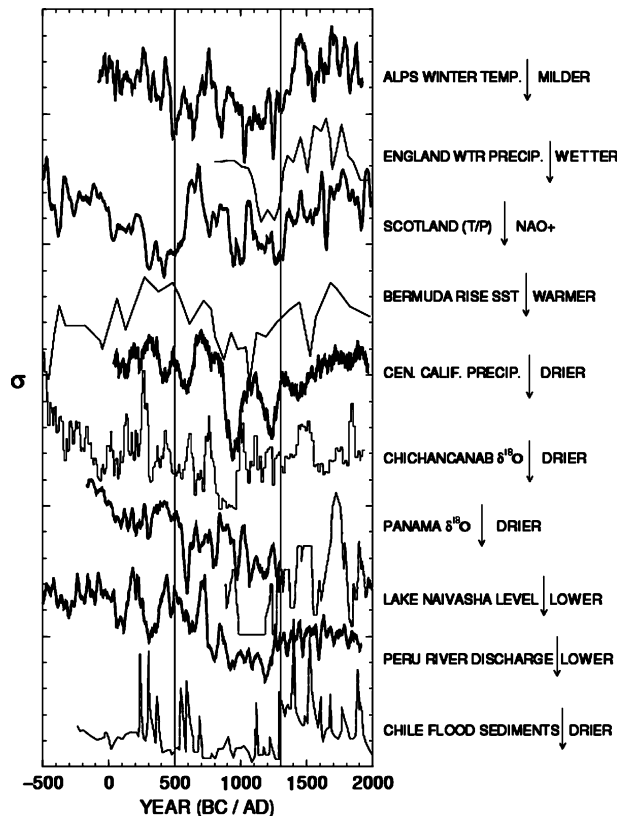


Fig. 13 a MCA vs. MODERN simulation differences for November–March conditions from the CCM3 experiments for 500 hPa heights (m, *bottom left*), precipitation (difference as percent of MODERN simulation value, *top left*), and surface air temperature (C, *top right*). Contour intervals are 10 m, 10% and 0.4 C, respectively. b As in panel a, but for March–June

considerable similarity to some of those shown earlier from the tropical Pacific and western US is the speleothem $\delta^{18}\text{O}$ record from Spannagel Cave in the Austrian Alps (Mangini et al. 2005; see Table 1; Fig. 14). Using a calibration of this isotopic record against reconstructed annual average Alps temperature (derived from historical records back to 1500; Luterbacher et al. 2004), Mangini et al. suggest that high altitude (~2,400 m) MCA alpine temperatures were relatively warm, averaging 1.7°C above LIA values and about the same as present-day values. Basing their argument on modern measurements of isotopic concentrations in Alpine meteoric water, Mangini et al. hypothesize that the apparent temperature signal in speleothem $\delta^{18}\text{O}$ reflects changes in the seasonal timing, trajectories and source regions of the air masses from which regional precipitation derives [less depleted in summer than winter, and for more marine (south and west) than more continental (north and east) trajectories]. One possibility that arises from this line of reasoning is that the MCA-LIA fluctuations in Spannagel $\delta^{18}\text{O}$ may record changes in the strength of the winter westerlies across Europe, often described through changes in the North Atlantic Oscillation [NAO, an index of the meridional SLP gradient across the North Atlantic, e.g., Hurrell (1995)], with Alps precipitation becoming isotopically lighter when the westerlies are relatively strong and NAO index is high. Interpreted in this light, the Spannagel record would indicate stronger cool season westerlies across Europe during the MCA (high NAO Index), a pattern associated with warmer temperatures and higher precipitation across northern Europe. As can be seen in Fig. 14, the timing of the changes in the Spannagel record closely follow those from the tropical and mid-latitude Pacific (cf. Fig. 7), and from the western US

Fig. 14 Geographically distributed proxy records that show MCA-LIA variability like seen in the western US and tropical Pacific (compare with Figs. 3, 4 and 7). The England winter precipitation, Bermuda Rise SST, Lake Naivasha level, and Chile flood deposition [Laguna Aculeo, after Jenny et al. (2002)] records are unsmoothed, the Alps winter temperature (Spannagel Cave), Scotland (Uamh an Tartair Cave) T/P, temperature/precipitation, Panama (Chilibrillo Cave) $\delta^{18}\text{O}$, Peru (core SO147-106KL) river discharge and central California PDSI records are smoothed over sliding 25-year, the Laguna Chichancanab $\delta^{18}\text{O}$ record over 51-year windows. Values are standard deviations (σ) for the smoothed records over the period of record shown; vertical axis tick marks are separated by 1σ



(cf., Figs. 3 and 4), indicating that the MCA epoch of cool (eastern) tropical SSTs and strong (winter) high pressure over the eastern North Pacific may also have been marked by a generally high NAO Index. A possible mechanism for this correspondence is examined later. [Note: the inference that the Spannagel record represents cool season rather than warm season temperatures is supported by the correlation between 25-year block-averaged Spannagel $\delta^{18}\text{O}$ (with an age adjustment of 20 years) and reconstructed Alps winter temperature since 1500 (area-average from the data of Casty et al. 2005; cf. Mangini et al. 2005, their Fig. 4) is 0.61, while for summer temperature the correlation is -0.05 (the correlation with reconstructed winter precipitation from the Casty et al. data is 0.05).

The suggestion of enhanced winter westerlies across northern Europe is finds some (though not complete) support in other records. For example, the reconstruction of England winter precipitation from Lamb (1965; the first description of a Medieval climate anomaly; Fig. 14) shows high winter precipitation (indicating a high NAO) during latter part of the MCA decreasing rapidly at about 1300 A.D., in close agreement with the timing seen in the Spannagel isotopic record. The idea of a high winter MCA NAO index and enhanced westerlies has also posited by Pfister et al. (1998) in relation to (relatively sparse) historical evidence (and perhaps most persuasively on the basis of horticultural accounts) for relatively mild MCA European winter temperatures, or at least relatively rare incursions of Arctic air masses (cf. Lamb 1965, 1977; Alexandre 1987). Similarly, the historically-based Low Country winter temperature reconstruction of van Engelen et al. (2001) (also Shabalova and van Engelen 2003; note that this record and those of Alexandre and Pfister et al. are not completely independent) is sparse before about 1300 A.D. and is ambivalent on the question of a MCA winter temperature in western Europe. The interpretation of the pre-1300 portion this latter record can be altered entirely depending on whether “absence of evidence” of any kind (i.e., no reports of severe or mild winters) is interpreted as suggesting infrequent severe winters (if it is not, the record is simply sparse and distinctive mostly in indicating frequent severe winters during the 10th century; if it is, the record suggests generally mild MCA winters and, perhaps coincidentally, closely resembles the Scotland and Austrian Alps speleothem records described below).

Proxy evidence supporting enhanced MCA westerlies over northwestern Europe is provided by the speleothem record from Uamh an Tartair (cave) in northwest Scotland (Fig. 14; Proctor et al. 2000, 2002). Calibrating with regional precipitation and temperature records, these authors show that speleothem growth rate is closely associated with the temperature-precipitation ratio and argue that growth rate changes through the late Holocene have been governed principally by precipitation variability (which is strongly correlated over Scotland with the NAO). If this interpretation is correct, then the wet MCA winters in Scotland and England indicated by the Uamh an Tartair record and Lamb’s (1965) reconstruction, and the light isotopic signature in the Spannagel record, are common signatures of enhanced winter westerlies, increased fluxes of Atlantic moisture into Europe, and a higher NAO index during the MCA.

One of the records often used to portray the timing and character of MCA-LIA climate change (e.g., deMenocal et al. 2000; Mangini et al. 2005) is the Bermuda Rise (Sargasso Sea) sediment core foraminifera $\delta^{18}\text{O}$ -based SST reconstruction (Keigwin 1996; see Table 1). This record (Fig. 14) indicates that annual average subtropical northwestern Atlantic SSTs were more than 1°C warmer than present during the MCA then decreased beginning in the eleventh century, in approximate correspondence with the general trend of the records shown in Fig. 14 (also Figs. 3, 4 and 7). Interestingly, modern SSTs in this region are strongly correlated with the NAO (e.g., Czaja and Frankignoul 2002; warmer SSTs when the NAO is positive).

Other widely cited instances of medieval climate variability are the 1 kyr BP Yucatan droughts that have been inferred to have had major cultural impacts on the Maya (e.g., Gill 2000). As exemplified by the Laguna Chichancanab ostracod $\delta^{18}\text{O}$ record (Fig. 14; Hodel et al. 1995, a proxy for evaporation-precipitation), proxy records from the region indicate a trend towards decreasing precipitation from 500 B.C. through the ninth and tenth centuries A.D., when a series of deep droughts apparently disrupted Classic Maya culture (e.g., Gill 2000). The general pattern of variability in this record is similar to others shown in Fig. 14 (and in Figs. 3, 4, and 6), and notably the period of severe Yucatan drought is coincides with the first of the deep MCA California droughts, as well as the beginning of the most extreme parts of the MCA in many records, including Palmyra and Peruvian coastal core SO147-106KL.

Haug et al. (2003) present evidence suggesting that particular periods of early MCA Yucatan droughts can be matched with specific periods of reduced river inflow into the southern Caribbean (i.e., reduced northern S. American precipitation). Using ^{14}C AMS-dated, biannually resolved titanium concentrations from a core from the Cariaco Basin (off eastern Venezuela; titanium is a proxy tracer for riverine sediment deposition; the high resolution record covers approximately 750–930 A.D.), these authors suggest a one-to-one correspondence between individual multi-year periods of inferred low river flow in Caribbean South America with specific Yucatan droughts described by Gill (2000) on the basis of archeological records (timing further supported by comparison between the Chichancanab and other lacustrine isotopic records with the Cariaco titanium record). While this evidence suggests temporal correspondence between several relatively dry multi-year periods in Yucatan and northern Venezuela, the Cariaco Basin titanium record clearly indicates that the MCA was relatively wet (in comparison to the LIA, and thus opposing the changes suggested in Yucatan) in northern Venezuela (including the Orinoco River basin), with substantial drying later from the early sixteenth through late nineteenth centuries (the timing of the latter being much like that seen Quelccaya record, see Peterson and Haug 2006).

The case for regional drying across Central America during the MCA is further supported by the well-dated (U-Th), high-resolution speleothem $\delta^{18}\text{O}$ record from Chilibrillo Cave in Panama (Fig. 14; Lachniet et al. 2004). The Chilibrillo record is consistent with that from Laguna Chichancanab in indicating general drying trend during the first millennium AD and particularly dry conditions during the MCA (extrapolation of the “modern climate” relationship between meteoric water $\delta^{18}\text{O}$ and precipitation amount in Panama to modern and MCA speleothem $\delta^{18}\text{O}$ suggests that long-term average MCA precipitation was about 20% less than the modern average). In addition, the Chilibrillo record shows excellent agreement with the Haug et al. (2003) data [cross-correlations between the two records (both smoothed with 11-year running means) peak sharply at 0.54 at a lag of 3 years; not shown]. It is unfortunate that the Chilibrillo record ends in 1310 A.D., near where many records would place the close of the MCA, but up to that point the record shows no indication of a downward trend in $\delta^{18}\text{O}$ (increasing precipitation); however, the record does provide additional evidence for a relatively dry MCA in portions of Central America.

These associations argue for generally dry conditions and instances of regional decadal-scale drought during the early MCA across southern Caribbean and Central America. The similarity in the general timing of the records from this region and the others described here suggests the possibility of common causal factors for the Yucatan droughts and other MCA extremes. At the same time, it is worth noting that modern Yucatan precipitation shows little association with tropical Pacific SSTs or with the NAO, nor does it exhibit strong correlations with SSTs in nearby regions (the same is true in the CCSM and MPI coupled

model results). Further complicating the interpretation of a dry MCA in Central American and southern Caribbean within the context of evidence for cool tropical Pacific SSTs is the fact that the modern climate record shows a clear inverse association between northern South American and southern Central American precipitation and eastern tropical Pacific SSTs (Estoque et al. 1985; Poveda and Mesa 1996; Ropelewski and Halpert 1987; George et al. 1998; Enfield and Alfaro 1999).

Also shown in Fig. 14 is the reconstructed record of lake level from Lake Naivasha (southwestern Kenya; Verschuren et al. 2000). This diatom- and chironomid-inferred (salinity proxies) reconstruction indicates that the level of this shallow, freshwater lake reached very low levels (<3 m; low rainfall) during the MCA, and increased to very high levels (>36 m; high rainfall) during the LIA. The timing of MCA-LIA transition agrees closely with many other records, as do some of the shorter time scale fluctuations (e.g., the Spannagel $\delta^{18}\text{O}$ record). During the October–December wet season (the “Short Rains,” one of two wet seasons in the region) central East African rainfall shows a modest positive association with eastern Pacific sea surface temperatures (e.g. Nicholson and Entekhabi 1987; Nicholson and Kim 1997). The precipitation changes underlying this relationship appear to be driven directly by altered Indian Ocean SST patterns (Goddard and Graham 1999), which in turn tend to fluctuate in concert with those in the central and eastern tropical Pacific (e.g. Turre and White 1995). For the “Short Rains” then, the apparent coincidence of cool eastern Pacific SSTs and decreased central East African precipitation during the MCA fits well with associations seen in modern climatology [and argues for a cool (warm) western (eastern) tropical Indian Ocean during the MCA]. (Note: In the modern climate, the February–April “Long Rains” are more reliable and not strongly connected with tropical Pacific variability (e.g., Ogallo et al. 1988; Rowell et al. 1994; Mutai and Ward 2000). While it is possible that the Long Rains played a (possibly dominant) role in MCA East African precipitation changes, it is not clear what signature such a correspondence would have with other far-field proxy records].

The final record shown in Fig. 14 is an index of flood sediment deposition (wet sediment density) from Laguna Aculeo from central Chile, near Santiago (Jenny et al. 2002). Austral winter half-year precipitation in central Chile is modulated by El Niño variability much as it is in the western US (but more strongly) with the probability of extreme precipitation events being considerably higher during warm episodes (Ropelewski and Halpert 1987; Grimm et al. 2000; for example, typical values of the linear correlation between NINO3 SST and austral winter average station precipitation in central Chile is 0.4–0.5). The Laguna Aculeo flood deposit record indicates low frequencies of high inflows after approximately 700 A.D. and a sharp increase at approximately 1300 A.D. The similarity between the timing and sharpness of the changes in this and those seen in several others discussed earlier (notably the Peru river flow reconstruction and several from the western US) argues for a common causal mechanism.

A winter European connection? A final set of analyses explores the possibility that cool tropical Pacific SSTs contributed to the tendency for warm and moist MCA winters in parts of northern and central Europe. As noted earlier, this hypothesis is suggested by the correspondence between European winter precipitation and temperature reconstructions (Fig. 14) and proxy records from the tropical Pacific and western US (Figs. 3, 4, 7, 14). The idea that changes in tropical Pacific SSTs could leave an imprint on European climate finds some support from analyses of instrumental period records (van Loon and Madden 1981; Fraedrich and Müller 1992; Pozo-Vázquez et al. 2001, 2005; Mariotti et al. 2002; Greatbatch et al. 2004) and has been explored in model experiments (Merkel and Latif

2002; Greatbatch et al. 2004; Brönnimann et al. 2004), and recently using historically-based reconstructions for the past 300 years (Brönnimann et al. 2006).

Fraedrich and Müller (1992), extending earlier work by van Loon and Madden (1981), Kiladis and Diaz (1989) and others, examined the response of SLP, temperature and precipitation over Europe (using station data) during 26 tropical Pacific “warm events” (El Niños) and 22 “cold events” (La Niñas) between 1880 and 1988. Their results, in large part consistent with earlier work, show a tendency for northern Europe to be cool and dry with high SLP during warm events with opposing conditions during cold events; southern and central Europe show the reverse response. Fraedrich and Müller go on to show (using daily surface weather charts and radiosonde data from 1952–89) that the observed response is due to southward (warm events) or northward (cool events) shifts in the preferred cyclone track and associated changes in the positions of large-scale circulation features across the northeast Atlantic.

These general results have been corroborated by subsequent studies of observed circulation and precipitation patterns, though studies covering the recent period suggest the response is not particularly systematic (Pozo-Vázquez et al. 2001, 2005; Greatbatch et al. 2004) and shows marked seasonality (Mariotti et al. 2002). Most recently, Brönnimann et al. (2006) studied the ENSO – European climate relationship through the past 300 years using field reconstructions of European precipitation and temperature and a several El Niño-related indices (historical and proxy). Their results show a clear response similar in most respects to those noted, including a relatively strong connection with the NAO (El Niño SSTs high, NAO low). Studies with atmospheric models (Merkel and Latif 2002; Brönnimann et al. 2004; Greatbatch et al. 2004) reproduce both the general characteristics seen in the studies noted above (precipitation, temperature and circulation patterns; preferred cyclone tracks), and reinforce the point that the specific results obtained (with regard to the impacts of El Niño and La Niña events) are sensitive to both averaging time (random effects) and the background states (e.g., extra-tropical Pacific SSTs), echoing van Loon and Madden’s (1981) point that the distance between the North Atlantic and Europe from the tropical Pacific makes it “...not surprising if at times the influence of the oscillation is superseded by other effects.”

In the context of the remarks above, Fig. 15 shows differences in North Atlantic and European December–March 2-meter temperatures and 500 hPa anomalies between the results of the CCM3 MCA and MODERN experiments described earlier (see Fig. 13a, b). The results show MCA warming over northern and central Europe, with 2-m temperature anomalies of 0.6–1.0°C over much of northwestern Europe and reaching 1.6°C over the Urals. This pattern is accompanied by the familiar signature of a positive NAO pattern in the 500 hPa anomaly field. Other analyses (not shown) using area-averaged temperatures (50–70N, 5–50E) show these (20 member ensemble) differences are significant well above the 99th percentile. This basic result is qualitatively repeated in the PSR MCA-LIA composite difference maps (Fig. 16) for the CCSM and MPI coupled model results formed (as in Figs. 11 and 12) on the basis of (1) tropical Pacific SSTs, or (2) California precipitation and SSTs. Each of these composite difference maps shows warmer MCA temperatures over northern Europe (1.6–2.0°C maximums; generally reaching farther west and south in the MPI results) and patterns of SLP change that produce increased westerly flow across northern Europe. These changes are associated with increases in inferred MCA precipitation of 5–10% over northwestern Europe (not shown), consistent with values obtained for modern climate by Pozo-Vázquez et al. (2005).

To illustrate the relationship between tropical Pacific SSTs and European winter temperatures in the simulations more clearly, Fig. 17 shows scatter plots of December–

Tref and H500: CCM3 MCA – MODERN

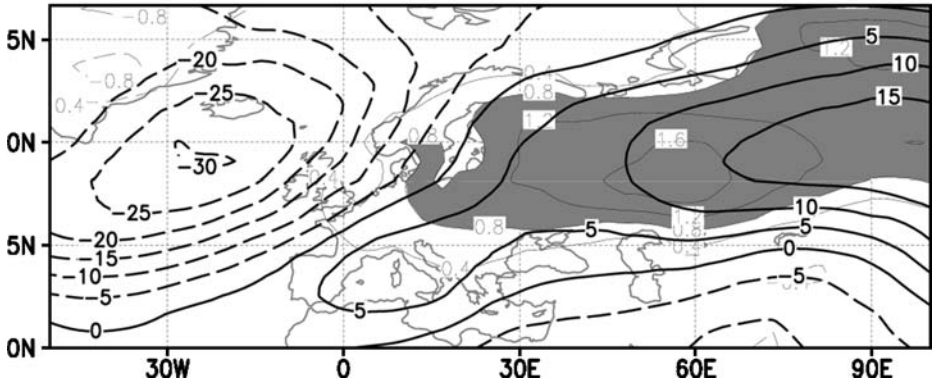


Fig. 15 Ensemble mean differences in December–March average surface air temperature ($^{\circ}\text{C}$, *thin contours*, contour interval 0.4 $^{\circ}\text{C}$; *shading* indicates differences larger than 0.8) and 500 hPa heights (m, *heavy contours*; contour interval 5 m) between the CCM3 MCA and MODERN simulations

March northern European 2-m temperature (5–50E, 50–70W) vs. NINO3.4 SST anomalies from the CCSM and MPI results. When stratified according to NINO3.4 SST and aggregated over 15 sample blocks, the negative relationship for both models is clear and indicates a decrease of 0.6–0.8 $^{\circ}\text{C}$ in northern European temperature per 1.0 $^{\circ}\text{C}$ increase in NINO3.4 SST. At the same time note that the correlations between the raw December–

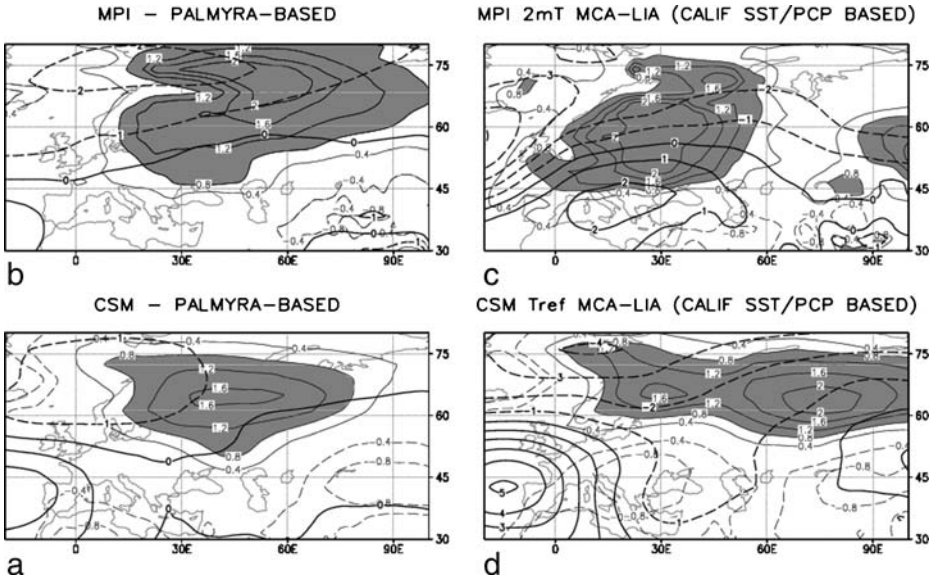
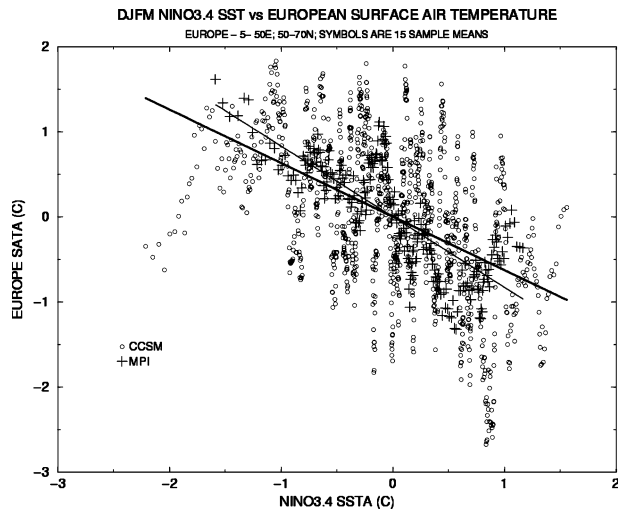


Fig. 16 Differences in December–March average surface air temperature ($^{\circ}\text{C}$; *thin contours*, contour interval 0.4 $^{\circ}\text{C}$; *shading* indicates differences larger than 0.8) and SLP (hPa; *heavy contours*; contour interval 1 hPa) from PSR-derived composites. Plots on the right-hand side (panels C and D) are from the California proxy SST-precipitation PSR composites (as in Fig. 11a, and b) and show differences between averages for 950–1250 A.D. less those for 1550–1850 A.D. *Left* hand panels (A and B) show differences from the Palmyra coral NINO3.4 PSR composites (as in Fig. 12a, b) and show differences for available portions of the Palmyra record between averages for 928–1220 A.D. (106 available years) less those for 1317–1703 A.D. (116 available years). *Lower* panels (A and D) show CCSM model results; *upper* panels (B and C) show MPI model results

Fig. 17 December–March northern European surface air temperature anomalies (5–50E; 50–70N) plotted as a function of NINO3.4 SST anomaly from the CCSM (light circles) and MPI (crosses) simulations; plotted values are 15-sample averages from the data ordered according to NINO3.4 values. Heavy (thin) lines show linear regression fits

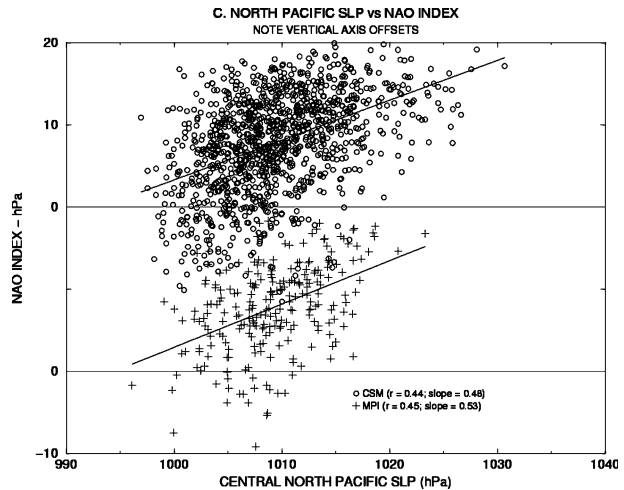


March average NINO3.4 and northern European temperature series for these models are quite modest, -0.23 for CCSM ($n=1150$) and -0.31 for MPI ($n=240$), emphasizing the point of van Loon and Madden (1981) regarding the relative weakness of the response to tropical Pacific SST variability over the North Atlantic and Europe. Nevertheless, as can be seen in Figs. 16 and 17, averaging over many realizations reveals a substantial effect. This same averaging effect would explain why a tropical Pacific–European relationship, one that is relatively weak at interannual time scales, would appear robustly at centennial time scales given low frequency changes in forcing.

Given the results above, it is not surprising that a similar degree of association is found in between central California precipitation and European winter temperature (not shown) from the CCSM and MPI results, with correlations for December–March averages of -0.23 for CCSM, -0.25 for MPI (sample sizes as above). This result is consistent with the association between, for example, the Spannagel $\delta^{18}\text{O}$ record and the California precipitation (and fire-related) proxy records. Likewise, scatter plots of simulated central North Pacific SLP (area-average 130–170W, 35–50N) vs. the NAO (difference in area-averages for 20W–80W, 35–50N and 20E–80W, 60–80W) from the two coupled models (Fig. 18) show a systematic positive association (correlations of 0.38 and 0.48 for CCSM and MPI, respectively). The relative strength of the relationship between these two mid-latitude circulation indices suggests the possibility that the similarity between western US, tropical Pacific and European proxy records at centennial (MCA to LIA) timescales reflects a time-averaged “distillation” of favored low wavenumber configurations in the Northern Hemisphere westerlies [as implied by Figs. 11 and 13 (northeast Pacific/North America) and Figs. 15 and 16 (northeast Atlantic/Europe)] which are, in turn, controlled to some degree by changing tropical Pacific SSTs.

The interpretation outlined above requires a note of caution. As in observations (e.g. Greatbatch et al. 2004), the associations obtained using the coupled model results can change in the magnitude depending on the temporal filtering that is applied. For example, for the MPI simulation (which is relatively short and has little centennial variability), the association between NINO3.4 and northern European temperature becomes stronger ($R=-0.52$; significance level $>95\%$ by Fisher’s z -transform) when the records are smoothed with a 15-year running mean. For the CCSM simulation, which has substantial centennial-scale

Fig. 18 NAO index plotted as a function of central North Pacific SLP from the CCSM and MPI simulations. The NAO index is defined (as in Hurrell 1995) as the difference between area-average SLP (hPa) in the regions 80W–20E, 30–50N and 80–20W, 60–80N; central North Pacific SLP is the area-average for 170–130W and 35–50N. Plotted values are individual (unsmoothed) December–March averages. The two distributions are offset by 20 hPa for the NAO (*vertical axis*) for clarity



temperature variability (see Section 2), the association between NINO3.4 SST and northern European temperature disappears when each is smoothed with a 15-year running mean. When the same exercise is applied to the California precipitation and European temperature series, the relationships for both models retain the same sense, but are weakened. On the other hand, for both models the correlations between central North Pacific SLP and the NAO are strengthened to between 0.5 and 0.6 in both models when the 15-year running mean is applied. These results emphasize the point that different sorts of boundary-forced climate variability can produce different frequency- and variable-dependent responses in different variables, even in the “perfect data” world of climate simulations.

4 Summary and discussion

This foregoing presentation is divided into two main parts. The first presents a comparative review of a variety of proxy records and reconstructions bearing on MCA climate change in the western US and the tropical Pacific. The second frames the patterns of variability seen in these records (and some others from widely distributed locations) within the context of the hypothesis that cool tropical Pacific SSTs contributed to some defining attributes of MCA climate.

The results of the first part reprise evidence for the long established view of the medieval centuries as a time of recurrent deep drought in the western US (LaMarche 1974; Stine 1994) and describe some new evidence suggesting that average MCA conditions in the tropical Pacific resembled those experienced during extreme La Niña conditions in the modern climate. The findings in the second part show that cool tropical Pacific SSTs are consistent with MCA climate change inferred from the proxy records in the western US and (more tenuously) in other regions as well.

The review of the proxy records for western North America given here is not exhaustive but hopefully complimentary to much more complete analyses (some referred to in the text) that examine specific records in detail, many of which provide comparisons with other records as well. A notable gap in this presentation is discussion of evidence for MCA drought in the central US. There is considerable literature relating to this topic, much of it

covering evidence for MCA dune mobilization and lacustrine reconstructions of salinity and eolian deposition. Examples of the former include Muhs (1985), Arbogast (1996), Muhs et al. (1997), Holliday (2001) and Mason et al. (2004) who describe the evidence for dune mobilization in the western Great Plains from northern New Mexico to North Dakota, generally in the period 800–1300 A.D. (cf. Forman et al. 2001 for a general review). Largely consistent inferences are drawn from the continental lacustrine records. For example, the Elk Lake (Minnesota; Dean 1997) record shows large peaks in quartz deposition during the eleventh and twelfth centuries (indicating soil mobilization and/or eolian deposition) and elevated fractional populations of the diatom *M. granulata*, suggesting increased wind mixing. Consistent with this timing, peaks in salinity (indicating precipitation deficits) appear at about the same time in both the Elk Lake (Laird et al. 2003) and Moon Lake (Minnesota; Laird et al. 1998) records (interestingly, records from nearby lakes to the north show different behavior, suggesting a perspective of the mid-continent MCA droughts as shifts in climatic gradients, rather than continental-scale features).

When considering the central hypothesis of this paper (a relatively cool MCA tropical Pacific), it should be noted that two prominent proxy records related to tropical Pacific variability show behavior apparently inconsistent with generally cool SSTs in the eastern tropical Pacific during the MCA. These include the Quelccaya ice cap $\delta^{18}\text{O}$ and accumulation records (Peru; Thompson et al. 1984, 2000) and Laguna Pallcacocha sediment record (Ecuador; Rodbell et al. 1999; Moy et al. 2002). With regard to the Quelccaya record, there is good evidence based on other Andean ice cores, in situ data, modeling results and meteorological considerations that there is a shared isotopic signal in some different cores over past centuries and b) that the imprint of modern El Niño variability is recorded in tropical Andean ice cap isotopic concentrations (Garreaud and Aceituno 2001; Vuille et al. 2003a,b; Bradley et al. 2003b; c.f. Hoffmann et al. 2003; Seimon 2003), and probably in accumulation as well (Hardy et al. 2003). It is notable then that the Quelccaya $\delta^{18}\text{O}$ record (not shown) shows little multi-centennial change in $\delta^{18}\text{O}$ during the MCA, with major decreases beginning in the early sixteenth century reaching a minimum in the early nineteenth century. If it is assumed that the Quelccaya $\delta^{18}\text{O}$ record responds principally to changes in eastern tropical Pacific SST, not only is the sense of this change opposite to that expected on the basis of warming SSTs during the LIA, but the sixteenth century shift occurs two to three centuries after the MCA-LIA transition as seen in many other records. A further conflicting issue is that the Quelccaya accumulation record (not shown) neither resembles the (inverted) $\delta^{18}\text{O}$ record, nor the character and timing of MCA climate changes suggested by Palmyra coral or Peruvian riverine deposit records (and others shown in Fig. 7). A possible explanation for these apparent inconsistencies may be that although the isotopic content of meteoric water at Quelccaya is modulated by El Niño-related changes in atmospheric circulation and stability (Garreaud and Aceituno 2001; Vuille et al. 2003a), the source region for Quelccaya precipitation is the tropical Atlantic (Thompson et al. 2000; Vuille et al. 2003a,b). Thus, the Quelccaya $\delta^{18}\text{O}$ and accumulation records may reflect the influence of a variety of factors (including tropical Atlantic SSTs) that are preferentially reflected at different time scales [in this regard it is of interest to note that the post-MCA Quelccaya $\delta^{18}\text{O}$ record resembles aspects of the reconstructed SST record from off northeast Africa (de Menocal et al. 2000)].

The sediment core record from Laguna Pallcacocha near the crest of the Ecuadorian Andes (Moy et al. 2002; c.f., Rodbell et al. 1999) contains light-colored laminae marking the deposition of clastic material into the lake and its watershed during high rainfall events which are expected to occur more frequently during El Niño episodes (c.f. Graham 2004). However, the variability in the Pallcacocha record (not shown) during MCA and LIA is

difficult to interpret. During the MCA, total clastic deposition rates are high but the frequency of high amplitude events is relatively low; in contrast, after the fourteenth century (going into the LIA), deposition rates decrease sharply and the frequency of high amplitude events increases. The timing of these changes is in approximate agreement with the MCA-LIA transition seen in other records, but as with the Quelccaya record, the record seems ambiguous with regard to MCA and LIA conditions in the tropical Pacific. Whether the Quelccaya and Pallacocha records argue conclusively against La Niña-like conditions in medieval times, or whether other processes (affecting isotopic variability and sediment deposition patterns in the equatorial Andes) mask the effects of a cool MCA tropical Pacific in these records, is a matter that must await future findings to be resolved.

It is worthwhile to consider the relative confidence that should be assigned to ideas that have been presented. First, the evidence for an arid MCA in the western and central US with severe century-scale regional droughts is compelling. There seems little doubt that multi-decadal periods saw decreases in regional California precipitation on the order of 15–25%, with much more severe conditions lasting a decade or more. To frame the severity of these MCA droughts in the context of modern precipitation variability, the 50-year periods beginning in 906 and 947 A.D. (calculated from non-overlapping blocks starting 47 A.D.) were the two driest in the reconstructed California Division 6 record, registering 73 and 76% of the reconstructed average for 1886–97 (the calibration period), respectively. The corresponding values for the 50-year periods beginning 1897 and 1947 are 106 and 95%. Six of the 10 driest (independent) decades in that record occurred during the century beginning in 897 A.D., these ranging from 62 to 75% of the long-term mean; in comparison, the decades beginning in 1897 A.D. had a corresponding range of 85% (1947) to 126% (1937, third wettest in the reconstructed record). Hughes and Funkhouser (1998) provide a similar perspective from the Great Basin, for example, only one, two and four, respectively, of the 10 driest 50-, 20- and 10-year periods since AD 234 occurred after 1500 A.D., and none occurred in the twentieth century. The first, second and first driest, respectively, 50-, 20- and 10-year periods occurred in the tenth century, and were conservatively estimated to be of the order of 88, 84 and 77% of the instrumental mean. These periods of medieval drought in California, the Great Basin, and western US in general were remarkable not only for aridity but for persistence (Stine 1994; Cook et al. 2004; Graham and Hughes 2007) and were undoubtedly accompanied by pronounced changes in winter and spring circulation patterns over (at least) the North Pacific and North America (cf. Seager et al. 2005; Herweijer et al. 2006; Sridhar et al. 2006). [Note: while our analyses for the western US concentrate on boreal winter and spring MCA precipitation deficits, some evidence suggests that medieval times saw increased in summer precipitation in the interior southwestern US (e.g. Petersen 1988, 1994; Davis 1994; Wigand and Rhode 2002)].

Direct evidence for La Niña-like conditions in the tropical Pacific during the MCA is intriguing, but not as compelling as that for arid conditions in the western US. At present, the case rests largely on the Palmyra coral and Peru riverine sediment deposition records, with additional support from the Mindanao and Santa Barbara Channel SST reconstructions, and archeological evidence from coastal Peru discussed below. Important indirect evidence comes from close agreement between the timing in the tropical Pacific and western US and Chilean (Laguna Aculeo) proxy records, the physically consistent cross-proxy tropical-mid-latitude relationships, and the model-derived results suggesting that SST anomalies like those indicated by the Palmyra reconstruction would produce substantial reductions in precipitation in the western and central US (this paper and Herweijer et al. 2006). At the same time, the Quelccaya and Pallacocha records, at least according to their usual interpretation, appear inconsistent or ambivalent with the idea of a cool MCA tropical Pacific.

A connection has been tentatively drawn between the proxy and historical evidence for warm northern European winters during the MCA and the impacts of cool tropical Pacific SSTs on NH winter circulation. This latter suggestion is based on model results and observational studies presented here and elsewhere by others. The warmer MCA northern European temperatures result from increased winter west to southwesterly flow across the region (more positive NAO). A first point regarding this idea is that although there is some clear evidence for mild northern European winters during the MCA, it is but neither compelling nor well quantified in terms of magnitude, time or space (see discussions in Pfister et al. 1998; van Engelen et al. 2001; Proctor et al. 2002; Shabalova and van Engelen 2003; Mangini et al. 2005). With regard to a connection between northern European winter climate and tropical Pacific SSTs, observational and model-derived results show broad, but not uniform, consensus. That this association is not particularly strong and can thus be masked or altered by random effects or boundary conditions elsewhere (e.g., van Loon and Madden 1981; Greatbatch et al. 2004; Hurrell et al. 2004; Hoerling et al. 2004). Whatever the forcing mechanism, our results and others (e.g. Brönnimann et al. 2004) suggest a tendency for an association between ridging (troughing) over the central North Pacific and a positive (negative) NAO index, a result quite consistent with the MCA-LIA association between dry (wet) conditions in the western US and mild (cold) European winters inferred (tentatively) from proxy and historical reconstructions.

A major part of the initial motivation for this work arose from recognition of the approximate coincidence between the cooling coastal SSTs found the Santa Barbara Basin SST reconstruction) and increasing MCA aridity in California (Kennett and Kennett 2000). This finding arises within the context of the archeological perspective linking medieval drought with increasing violence and the emergence of institutionalized social hierarchies in the Santa Barbara region of central/southern California (e.g., Arnold 1992, 1997; Raab and Larson 1997; Jones et al. 1999; Kennett and Kennett 2000). These authors present evidence supporting a scenario in which reduced availability of water and changes in marine productivity favored societal organization more focused on defense of resources and more organized division of labor.

Archeological records elsewhere also suggest a link between cultural shifts and MCA climate changes. Well known examples of such suggested links include the apparent impact of drought on the Tiwanaku near Lake Titicaca during the latter part of the MCA (Binford et al. 1997) and the previously noted evidence concerning the Maya in Yucatan (Gill 2000). The case for climate-culture interactions has also been argued for Moche, an advanced culture that evolved during the first millennium A.D. along the north-central coast of Peru, in part through the construction of sophisticated irrigation works to help manage the flow from westward flowing rivers fed by Andean highland precipitation. These works included reservoirs in the Andean foothills and stone-lined canals that conveyed water from the reservoirs to agricultural centers in coastal valleys up to 25 km away (e.g., Kosok 1940; Farrington and Park 1978; Nials et al. 1979a,b). Moche culture flourished between approximately 300 and 600 A.D., and underwent a major reorganization late in that period (Nials et al. 1979a,b; Moseley et al. 1981; Moseley and Deeds 1982; Shimada et al. 1991; Dillehay and Kolata 2004). This reorganization included the occupation of more northerly sites and inland centers near the canal intakes, apparent abandonment of more southerly centers, and a general decline in the development of sophisticated infrastructures. Shimada et al. (1991; cf. Dillehay and Kolata 2004), have suggested that the transition marks the cultural response to an extended drought (563–594 A.D.; see Fig. 19) inferred from the Quelccaya accumulation record.

Although dating uncertainties preclude convincing comparison with the Shimada et al. (1991) chronology for sixth century Moche transition and Quelccaya accumulation-inferred

drought, it is of interest that the Peruvian river sediment discharge reconstruction (Rein et al. 2004, 2005) portrays the period of Moche development as one of amplifying precipitation variability. This variability may be reflected in the widespread evidence of damage to irrigation systems and agricultural lands from flooding and dune encroachment around the fourth century (Moseley et al. 1981; Moseley and Deeds 1982; cf. Shimada et al. 1991) Further, and particularly intriguing, is the apparent coincidence between the abrupt disappearance of Moche “as a distinctive cultural phenomenon” (Dillehay and Kolata 2004) at about 800 A.D. and the abrupt collapse of riverine sediment deposition as seen in the Peruvian coastal core (SO147-106KL) data at the entry into the very dry conditions of the MCA proper (Fig. 19).

During the post-Moche period, Chimú culture developed slowly and by 1200 A.D. dominated the northern Peruvian coastal region as an advanced society until being absorbed by the Incas during the fifteenth century (Dillehay and Kolata 2004). It is not clear whether there is a climatic connection between Chimú ascendancy and the twelfth century MCA-to-LIA transition indicated in the SO147-106KL record (and others at about the same time), but the impact of (apparently) El Niño-related lowland precipitation events is apparent in geological and archeological evidence from this time (Dillehay and Kolata 2004), as it is for the Moche period, in the evidence of both dune mobilization (late thirteenth century) and flash flooding. As shown in Fig. 19, the timing of the Chimú flood events matches closely with the onset of the LIA indicated by the SO147-106KL record and others from western North America (see Figs. 3 and 4).

In geographical counterpoint to the contemporaneous evolution of Chimú culture in northern Peru, Nunn (2000) reviews a suite of evidence for sharp cultural and environmental changes in the western tropical Pacific at the MCA-LIA transition, identified

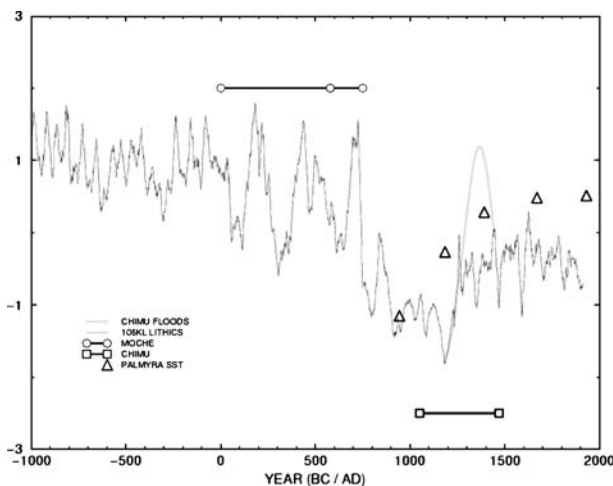


Fig. 19 Northern Peru River sediment discharge reconstruction (SO147-106KL lithics; *solid curve*; standardized running 25-year block means) and Palmyra coral reconstructed NINO3.4 SSTA (*triangles*; C; segment averages). *Solid horizontal line with circles* shows approximate duration of Moche culture in north-central coastal Peru (*center circle* marks approximate center of 563–594 A.D. drought inferred by Shimada et al. (1991)). *Solid horizontal line with squares* marks approximate duration of Chimú culture. *Gray curve* shows aggregate probability distribution (arbitrarily scaled) of calibrated AMS ^{14}C dates for late twelfth–mid-fifteenth century A.D. floods for flash floods affecting the Chimú region [from Table 1 of Dillehay and Kolata (2004)]

as “the A.D. 1300 event” by regional archeologists and paleo-scientists. If the Palmyra SST reconstruction and SO147-106KL record are taken at face value, the scale of climate change in this region would have been comparable to the well documented socially and ecologically disruptive effects of a switch from modern La Niña to El Niño conditions, with a good deal of the shift taking place in perhaps a century. In the western tropical Pacific, these climatic effects would include major changes in precipitation distributions (e.g., Figs. 12 and 13), altered wind patterns and decreased sea level. In this regard, it is noteworthy then that Nunn’s (2000) review includes a number of citations for evidence of decreasing sea level in that region dated to 1300–1400 A.D. Nunn (2000) also notes that the period of long-distance voyaging in the western Pacific at about 1300 A.D., approximately contemporaneous with the apparent MCA-LIA transition. The suggestion of a connection with climate change for this cultural shift has been raised previously (Bridgeman 1983; Finney 1985; Nunn 1994), and is a topic that might fruitfully be reevaluated.

Much of wide-ranging physical and cultural evidence for MCA-LIA Pacific climate change described by Nunn (2000) is difficult to frame neatly (in terms of geography, timing, or magnitude) within the context of the scenario for decreasing tropical Pacific zonal SST gradients during the twelfth–fourteenth centuries suggested by the proxy records described earlier. Although some of the evidence cited by Nunn (2000) is open to alternative interpretation, much of it is qualitatively consistent with a shift from an MCA La Niña-like state to something more like modern conditions; certainly the timing of “around 1300 A.D.” for the western Pacific environmental and cultural changes is provocative in itself.

The nexus between long-established evidence for medieval drought in the western US (and perhaps in mid-latitude Chile) and recent evidence suggesting a cool tropical Pacific may provide a causal mechanism for the former and support for the reality of the latter. It also offers a partial response to the query posed by Hughes and Diaz more than a decade ago (Hughes and Diaz 1994), if not a “Medieval Warm Period,” then a substantial “Medieval Climate Anomaly,” a significant transient in Holocene climate that affected a large area of the Pacific Sector during medieval time, from about 500–1300 A.D. In addition, this synergy in cause and effect makes suggestions of some of the more distant climate effects from altered tropical Pacific SSTs more plausible (on dynamical grounds) and may afford opportunities to better understand other aspects of MCA climate change.

While the near-global scale of MCA climate change seems to be becoming more apparent, important questions remain concerning Late Holocene climate. The foremost among these concerns the state of the tropical Pacific in medieval times. Fortunately, yet to be analyzed fossil corals exist that may well go far towards resolving this question. Other questions concern the inconsistencies and gaps in the climate record – these might be filled by new, well quantified, proxy records of particular interest (e.g., of low latitude Indian Ocean and Atlantic SSTs, European winter temperature, Indo-Pacific precipitation, Meso-American precipitation). Other important questions concern mechanisms – for example, what changes in boundary conditions caused the apparent MCA boreal winter circulation shifts (if not tropical Pacific SSTs, then what)? and what processes could cause the tropical Pacific to cool substantially and then warm again centuries later? This latter topic has seen innovative initial work (Mann et al. 2005; c.f. Clement et al. 1996, 2000a,b) but requires further study.

Acknowledgments This work was supported by the NSF Earth System History program under NSF Grant ATM0213962 to MKH, NOAA Grant (NA06OAR4310120) to NEG, by the California Energy Commission PIER Program through the California Climate Change Center at Scripps Institution of Oceanography, and by the Hydrologic Research Center. Many people contributed to this work by providing data, information, and ideas – a hopefully inclusive list includes S. Anderson, A. Arbogast, R. Bradley, S. Brönnimann, L. Benson,

R. Byrne, D. Cayan, E. Cook, M. Dettinger, H. Diaz, O. Davis, J. Esper, M. Lachniet, J. Luterbacher, M. Mann, D. Meko, J. Mohr, M. Moseley, R. Seager, D. Stahle, S. Starratt, S. Stine, T. Swetnam, M. Vuille and E. Wahl. The authors also thank three anonymous reviewers whose comments assisted greatly in improving the manuscript.

Appendix

Description of Proxy Surrogate Reconstruction Method

Proxy Surrogate Reconstruction (PSR) is an analog method in which the temporal sequence of multi-variate output from a model simulation is reordered to obtain agreement between an index variable (\mathbf{Y}^*) from the model simulation with corresponding proxy data (\mathbf{Y} ; both \mathbf{Y} and \mathbf{Y}^* may be uni- or multivariate). The idea is to reorder the model output (the “surrogate” dataset) so that there is good serial agreement between \mathbf{Y} and \mathbf{Y}^* . When this is done, possible scenarios of past climate variability can be examined in any desired fields from the reordered model output. The methodology is outlined formally below.

- (1) Denote a proxy time series as $[t_i, \mathbf{Y}_i]$, where the t is the time index (e.g., corresponding to particular year) associated with the i th ($i=1, n$) record, and \mathbf{Y} is an arbitrary (possibly vector) element from a proxy reconstruction(s) (e.g., reconstructed Niño3 SST).
- (2) Denote corresponding time series from some surrogate data set (e.g. climate model output) as $[t_j^*, \mathbf{Y}_j^*]$, with ($j=1, m$). Note that the lengths of \mathbf{Y} and \mathbf{Y}^* are not necessarily the same. It is assumed that \mathbf{Y}^* bears some meaningful correspondence with \mathbf{Y} . Note that (as deemed appropriate) both \mathbf{Y} and \mathbf{Y}^* may be transformed expressions of the original proxy reconstruction and model values [i.e., $\mathbf{Y}=f(\mathbf{P})$ and $\mathbf{Y}^*=g(\mathbf{M})$].
- (3) Define a measure $S_{i,j}=h(\mathbf{Y}_i, \mathbf{Y}_j^*)$ that indicates the similarity between \mathbf{Y}_i and \mathbf{Y}_j^* (assume that smaller values of S indicate increasing similarity).
- (4) For each (proxy) element of \mathbf{Y}_i , select the member of \mathbf{Y}^* (from the surrogate data set) most similar to \mathbf{Y}_i (i.e., it has the minimum $S_{i,N}$) – call it $[\mathbf{Y}_k^*]$. Enter k as the i th member of an ordering vector, \mathbf{P} . When complete, \mathbf{P} defines a reordering of the surrogate data set constructed on the basis of the similarity (S) between \mathbf{Y} and \mathbf{Y}^* , and matching the time indices of the former (so that in the sense measured by S , $\mathbf{Y}_{\mathbf{P}(i)}^*$ corresponds to \mathbf{Y}_i).

As noted above, the record lengths of \mathbf{Y} and \mathbf{Y}^* need not be equal – if N is smaller than M , then the candidate data set will be sub-sampled, and if N is larger than M the candidate sample will be over-sampled (and the set $\mathbf{Y}_{\mathbf{P}}^*$ will contain repeated elements).

This technique has the advantages of allowing broad flexibility in the definition of “similarity,” and if the surrogate set is multi-variate model output (as in this paper), the cross-spatial and cross-variable relationships inherent in model physics are conserved. This last point allows suggestions to be entertained concerning the evolution of fields other than those directly involved in the construction of \mathbf{Y}^* . The method has the primary disadvantage of being relevant only where the range of \mathbf{Y} is covered by \mathbf{Y}^* , and of course is subject to assumptions concerning whether the relationship between the proxy and model indices (\mathbf{Y} and \mathbf{Y}^*) is meaningful, and their relationships to reality.

In this paper PSR is applied in two examples. In one case, \mathbf{Y} and \mathbf{Y}^* are 2-d vectors [model and proxy-based SST off south-central California and central California precipitation

(see Section 3.4.1). In a second application, \mathbf{Y} and \mathbf{Y}^* are scalars (model and proxy-inferred NINO3 SST). In both cases the measure of similarity (S) defined as the (Euclidean) distance between \mathbf{Y} and \mathbf{Y}^* .

References

- Alexandre P (1987) Le climat en Europe au moyen âge. Ecole des Hautes Etudes en Sciences Sociales, Paris
- Alexander MA, Scott JD, Deser C (2000) Processes that influence sea surface temperature and ocean mixed layer depth variability in a coupled model. *J Geophys Res Oceans* 105:16823–16842
- Ammann CM, Meehl GA, Washington WM, Zender CS (2003) A monthly and latitudinally varying volcanic forcing dataset in simulations of 20th century climate. *Geophys Res Lett* 30(12):1657–1659
- Ammann CM, Joos F, Schimel DS, Otto-Bliessner BL, Tomas RA (2007) Solar influence on climate during the past millennium: results from transient simulations with the NCAR Climate System Model. *Proc Natl Acad Sci* (in press)
- Anderson RS, Smith SJ (1997) The sedimentary record of fire in Montane Meadows, Sierra Nevada, California, USA. In: Clarke J, Cachier H, Goldammer JG, Stocks B (eds) *Sediment records of biomass burning and global change*, NATO ASI Series. Springer, Berlin Heidelberg New York, pp 313–328
- Arbogast AF (1996) Stratigraphic evidence for late-Holocene eolian sand mobilization and soil formation in South-Central Kansas, USA. *J Arid Environ* 34:403–414
- Arnold JE (1992) Complex Hunter-Gatherer-Fishers of prehistoric California: chiefs, specialists, and maritime adaptations of the Channel Islands. *Am Antiq* 57:60–84
- Arnold JE (1997) Bigger boats, crowded creekbanks: environmental stresses in perspective. *Am Antiq* 62:337–339
- Benson L, Kashgarian M, Dye R, Lund S, Paillet F, Smooth J, Kester C, Mensing S, Meko D, Lindström S (2002) Holocene multidecadal and multicentennial droughts affecting Northern California and Nevada. *Quat Sci Rev* 21:659–682
- Binford MW, Kolata AL, Brenner M, Janusek JW, Seddon MT, Abbot M, Curtis J (1997) Climatic variation and the rise and fall of an Andean civilization. *Quat Res* 47:235–248
- Bjerknes J (1966) A possible response of the atmospheric Hadley circulation to anomalies of ocean temperature. *Tellus* 18:820–829
- Bjerknes J (1969) Atmospheric teleconnections from the equatorial Pacific. *Mon Weather Rev* 97:163–172
- Boville BA, Gent PR (1998) The NCAR climate system model, version one. *J Climate* 11:1115–1130
- Boxt MA, Raab LM, Davis OK, Pope KO (1999) Extreme late Holocene climate change in coastal California. *Pac Coast Archaeol Soc Q* 35:25–37
- Bradley RS (2000) 1000 years of climate changes. *Science* 288:1353–1354
- Bradley RS, Hughes MK, Diaz HF (2003a) Climate in medieval time. *Science* 302:404–405
- Bradley RS, Vuille M, Hardy D, Thompson LG (2003b) Low latitude ice cores record Pacific sea surface temperatures. *Geophys Res Lett* 30(4):1174 doi:10.1029/2002GLO16546
- Bridgeman HA (1983) Could climate change have had an influence on Polynesian migrations? *Palaeogeogr Palaeoclimatol Palaeoecol* 41:193–206
- Brönnimann S, Luterbacher J, Staehelin J, Svendby T, Hansen G, Svenøe T (2004) Extreme climate of the global troposphere and stratosphere in 1940–42 related to El Niño. *Nature* 431:971–974
- Brönnimann S, Xoplaki E, Casty C, Pauling A, Luterbacher J (2006) ENSO influence on Europe during the last centuries. *Clim Dyn* (doi:10.1007/s00382-006-0175-z)
- Byrne R, Ingram BL, Starratt S, Malamud-Roam F, Collins JN, Conrad ME (2001) Carbon isotope, diatom, and pollen evidence for late Holocene salinity change in a brackish marsh in the San Francisco estuary. *Quat Res* 55:66–76
- Casty C, Wanner H, Luterbacher J, Esper J, Boehm R (2005) Temperature and precipitation variability in the European Alps since 1500. *Int J Climatol* 25:1855–1880
- Cayan DR, Dettinger MD, Diaz HF, Graham NE (1998) Decadal climate variability of precipitation over Western North America. *J Climate* 11:3148–3166
- Clement AC, Seager R, Cane MA, Zebiak SE (1996) An ocean dynamical thermostat. *J Climate* 9:2190–2196
- Clement AC, Seager R, Cane MA (2000a) Orbital controls on tropical climate. *Paleoceanography* 14:441–446
- Clement AC, Seager R, Cane MA (2000b) Suppression of El Niño during the mid-Holocene by changes in the Earth's orbit. *Paleoceanography* 15:731–737
- Cobb KM, Charles CD, Cheng H, Edwards RL (2003) El Niño/Southern Oscillation and tropical Pacific climate during the last millennium. *Nature* 424:271–276

- Cole KL, Wahl ER (2000) A late Holocene paleoecological record from Torrey Pines State Reserve, California. *Quat Res* 53:341–351
- Cook ER, Woodhouse C, Eakin CM, Meko DM, Stahle DW (2004) Long-term aridity changes in the Western United States. *Science* 306:1015–1018
- Czaja A, Frankignoul K (2002) Observed impact of Atlantic sea surface temperature anomalies on the North Atlantic Oscillation. *J Clim* 215:606–623
- Daniels ML, Anderson RS, Whitlock C (2005) Vegetation and fire history since the late Pleistocene for the Trinity Mountains, Northwestern California, USA. *Holocene* 15:1062–1071
- Davis O (1992) Rapid climate change in coastal Southern California inferred from pollen analysis of San Joaquin Marsh. *Quat Res* 37:89–100
- Davis O (1994) The correlation of summer precipitation in the Southwestern U.S.A. with isotopic records of solar activity during the medieval warm period. *Earth and Environmental Science* 26:271–287
- Dean W (1997) Rates, timing, and cyclicity of Holocene eolian activity in North-Central United States: evidence from varved lake sediments. *Geology* 25:331–334
- deMenocal P, Ortiz JD, Guilderson T, Sarnthein M (2000) Millennial-scale linkages between high- and low-latitude climate during the Holocene warm period. *Science* 288:2198–2202
- Dettinger MD, Cayan DR, Diaz HF, Meko DM (1998) North–South precipitation patterns in Western North America on interannual-to-decadal timescales. *J Clim* 11:3095–3111
- Dillehay TD, Kolata AL (2004) Long-term human response to uncertain environmental conditions in the Andes. *Proc Natl Acad Sci* 101:4325–4330
- Eber LE (1971) Characteristics of sea-surface temperature anomalies. *Fish Bull* 69:345–355
- Enfield DB, Alfaro EJ (1999) The dependence of Caribbean rainfall on the interaction of the tropical Atlantic and Pacific Oceans. *J Clim* 12:2093–2103
- Estoque MA, Luque J, Chandeck-Montzea M, Garcia J (1985) Effects of El Niño on Panama rainfall. *Geofis Int* 24:355–381
- Farrington IS, Park CC (1978) Hydraulic engineering and irrigation agriculture in the Moche Valley, Peru: c. A.D. 1250–1532. *J Archaeol Sci* 5:255–268
- Finney B (1985) Anomalous westerlies, El Niño, and the colonization of Polynesia. *Am Anthropol* 87:9–26
- Forman SL, Oglesby R, Webb RS (2001) Temporal and spatial patterns of Holocene dune activity on the Great Plains of North America: megadroughts and climatic links. *Glob Planet Change* 29:1–29
- Fraedrich K, Müller K (1992) Climate anomalies in Europe associated with ENSO extremes. *Int J Climatol* 12:25–31
- Garreaud RD, Aceituno P (2001) Interannual rainfall variability over the South American Altiplano. *J Clim* 14:2779–2789
- George RK, Waylen P, Laporte S (1998) Interannual variability in annual streamflow and the Southern Oscillation in Costa Rica. *Hydrol Sci J* 43:409–424
- Gill RB (2000) The great Maya drought: water, life and death. University of New Mexico Press, Albuquerque
- Goddard L, Graham NE (1999) Importance of the Indian Ocean for simulating rainfall anomalies over Eastern and Southern Africa. *J Geophys Res* 104:19099–19116
- Graham NE (2004) Late Holocene teleconnections between tropical Pacific climate variability and precipitation in the Western USA: evidence from proxy records. *Holocene* 14:436–447
- Graham NE, Hughes MH (2007) Reconstructing the Medieval Mono Lake low stands. (in review)
- Graumlich LJ (1993) A 1000-year record of temperature and precipitation in the Sierra Nevada. *Quat Res* 39:249–255
- Greatbatch RJ, Lu J, Peterson KA (2004) Non-stationary impact of ENSO on European winter climate. *Geophys Res Lett* 31 doi:10.1029/2003GL018432
- Grimm AM, Barros VR, Doyle ME (2000) Climate variability in Southern South America associated with El Niño and La Niña events. *J Clim* 13:35–58
- Grove JM (1988) *The Little Ice Age*. Methuen, London
- Hardy DR, Vuille M, Bradley RS (2003) Variability of snow accumulation and isotopic composition on Nevado Sajama, Bolivia. *J Geophys Res* 108 doi:10.1029/2003.JD003623
- Haug GH, Günther D, Peterson LC, Sigmon DM, Hughen KA, Aeschlimann B (2003) Climate and the collapse of the Maya civilization. *Science* 299:1731–1735
- Herweijer C, Seager R, Cook ER (2006) North American droughts of the mid-to-late nineteenth century: a history, simulation and implication for medieval drought. *The Holocene* 16:159–171
- Hodell DA, Curtis JH, Brenner M (1995) A possible role of climate in the collapse of the classic Maya civilization. *Nature* 375:391–394
- Hoerling MP, Kumar A, Zhang M (1997) El Niño, La Niña and the nonlinearity of their teleconnections. *J Climate* 10:1769–1786
- Hoerling MP, Hurrell JW, Xu T, Bates GT, Phillips AS (2004) Twentieth century North Atlantic climate change. Part II: understanding the effect of Indian Ocean warming. *Clim Dyn* 23:391–405

- Hoffmann G, Ramirez E, Taupin JD, Francou B, Ribstein P, Delmas R, Durr H, Gallaire R, Simoes J, Schotterer U, Stievenard M, Werner M (2003) Coherent isotope history of Andean ice cores over the last century. *Geophys Res Lett* 30(4):1179 doi:10.1029/2002GL014820
- Holliday VT (2001) Stratigraphy and geochronology of upper quaternary eolian sand on the southern high plains of Texas and New Mexico, United States. *Geol Soc Amer Bull* 113:88–108
- Hughes MK, Diaz HF (1994) Was there a “medieval warm period” and if so, where and when? *Clim Change* 26:109–142
- Hughes MK, Funkhouser G (1998) Extremes of moisture availability reconstructed from tree-rings from recent millennia in the Great Basin of Western North America. In: Beniston M, Innes JL (eds) *Impacts of climate variability on forests*. Springer, Berlin Heidelberg New York, pp 99–107
- Hughes MK, Graumlich LJ (1996) Climatic variations and forcing mechanisms of the last 2000 years, NATO ASI Series, vol 141: Multi-millennial dendro-climatic studies from the western United States, pp 109–124
- Hurrell JW (1995) Decadal trends in the North Atlantic Oscillation: regional temperatures and precipitation. *Science* 269:676–679
- Hurrell JW, Hoerling MP, Phillips AS, Xu T (2004) Twentieth century North Atlantic climate change. Part I: assessing determinism. *Clim Dyn* 23:371–389
- Jenny B, Valero-Gracés BL, Urrutia R, Kelts K, Veit H, Appleby P, Geyh M (2002) Moisture changes and fluctuations of the Westerlies in Mediterranean Central Chile during the last 2000 years: the Laguna Aculeo record (33°50'S). *Quat Int* 87:3–18
- Jones TL, Brown GM, Raab LM, McVickar JL, Spaulding WG, Kennett DJ, York A, Walker PL (1999) Environmental imperatives reconsidered. *Curr Anthropol* 40:137–170
- Kaplan A, Cane MA, Kushnir Y, Clement AC, Blumenthal MB, Rajagopalan B (1998) Analyses of global sea surface temperature 1856–1991. *J Geophys Res* 103:18567–18589
- Keigwin LD (1996) The little ice age and medieval warm period in the Sargasso Sea. *Science* 274:1504–1508
- Kennett DJ, Kennett JP (2000) Competitive and cooperative responses to climatic instability in coastal Southern California. *Am Antiq* 65:379–395
- Kiehl JT, Hack JJ, Bonan GB, Boville BB, Williamson DL, Rasch PJ (1998) The National Center for Atmospheric Research Community Climate Model: CCM3. *J Climate* 11:1131–1149
- Kiladis GN, Diaz HF (1989) Global climate anomalies associated with extremes in the Southern Oscillation. *J Climate* 2:1069–1090
- Kosok P (1940) The role of irrigation in ancient Peru. In: *Proc. 8th American scientific congress*, vol 2. Washington DC, USA, pp 168–178
- Lachniet MS, Burns SJ, Piperno D, Asmerom Y, Polyak VJ, Moy CM, Christenson K (2004) A 1500-year El Niño–Southern Oscillation history for the Isthmus of Panama from speleothem calcite. *J Geophys Res* 109 doi:10.1029/2004JD004694
- Laird KR, Fritz SC, Maasch KA, Cumming BF (1996) Greater drought intensity and frequency before AD 1200 in the Northern Great Plains, USA. *Nature* 384:552–554
- Laird KR, Fritz SC, Cumming BF (1998) A diatom-based reconstruction of drought intensity, duration, and frequency from Moon Lake, North Dakota: a sub-decadal record of the last 2300 years. *J Paleolimnol* 19:161–179
- Laird KR, Cumming BF, Wunsam S, Rusak JA, Oglesby RJ, Fritz SC, Leavitt PR (2003) Lake sediments record large-scale shifts in moisture regimes across the northern prairies of North America during the past two millennia. *Proc Natl Acad Sci* 100:2483–2488
- LaMarche VC (1974) Paleoclimatic inferences from long tree-ring records. *Science* 183:1043–1088
- Lamb HH (1965) The early medieval warm epoch and its sequel. *Palaeogeogr Palaeoclim Palaeoecol* 1:13–37
- Lamb HH (1977) *Climate: present, past and future*. Vol 2: climatic history and the future. Methuen, London, p 837
- Lau N-C (1985) Modeling the seasonal dependence of the atmospheric response to observed El Niños in 1962–76. *Mon Weather Rev* 113:1970–1996
- Long CJ, Whitlock C, Bartlein PJ, Millsaugh SH (1998) A 9000-year fire history from the Oregon Coast Range, based on a high-resolution charcoal study. *Can J For Res* 28(5):774–787
- Luterbacher JD, Dietrich E, Xoplaki E, Grosjean M, Warner H (2004) European seasonal and annual temperature variability, trends and extremes since 1500. *Science* 303:1499–1503
- Mangini A, Spötl C, Verdes P (2005) Reconstruction of temperature in the Central Alps during the past 2000 yr from a $\delta^{18}\text{O}$ stalagmite record. *Earth Planet Sci Lett* 235:741–751 doi:10.1016/j.epsl.2005.05.010
- Mann ME, Cane MA, Zebiak SE, Clement A (2005) Volcanic and solar forcing of the tropical Pacific over the past 1000 years. *J Climate* 18:447–456
- Mantua JN, Hare SR, Zhang Y, Wallace JM, Francis RC (1997) A Pacific interdecadal oscillation with impacts on salmon production. *Bull Am Meteorol Soc* 78:1069–1080
- Mariotti A, Zeng N, Lau K-M (2002) Euro-Mediterranean rainfall and ENSO – a seasonally varying relationship. *Geophys Res Lett* 29 doi:10.1029/2001GL014248

- Mason JA, Swinehart JB, Goble RJ, Loope DB (2004) Late Holocene dune activity linked to hydrological drought, Nebraska Sand Hills, USA. *Holocene* 14:209–217
- Meehl GA, Arblaster JM (1998) The Asian-monsoon and El Niño-Southern Oscillation in the NCAR climate system model. *J Climate* 11:1356–1385
- Mehring PJ, Wigand PE (1990) Comparison of late Holocene environments from woodrat middens and pollen: Diamond Craters, Oregon. In: Betancourt JL, Van Devender TR, Martin PS (eds) *Fossil packrat middens: the last 40,000 years of biotic changes*. University of Arizona Press, Tucson
- Meko DM, Therrell MD, Baisan CH, Hughes MK (2001) Sacramento River flow reconstructed to A.D. 869 from tree rings. *J Am Water Resour Assoc* 37:1029–1039
- Merkel U, Latif M (2002) A high resolution AGCM study of the El Niño impact on the North American/European sector. *Geophys Res Lett* 29 doi:10.1029/2001GL013726
- Millar CI, King JC, Westfall RD, Alden HA, Delany DL (2006) Late Holocene forest dynamics, volcanism, and climate change at Whitewing Mountain and San Joaquin Ridge, Mono County, Sierra Nevada, CA, USA. *Quat Res* 66:273–287
- Mitsuguchi T, Matsumoto E, Abe O, Uchida T, Isdale PJ (1996) Mg/Ca thermometry in coral skeletons. *Science* 274:961–963
- Mohr JA, Whitlock C, Skinner CN (2000) Postglacial vegetation and fire history, Eastern Klamath Mountains, California, USA. *Holocene* 10:587–601
- Moseley ME, Deeds EE (1982) The land in front of Chan Chan: agrarian expansion, reform, and collapse in the Moche Valley. In: Moseley M, Day K (eds) *Chan Chan: Andean Desert City*. University of New Mexico Press, Albuquerque, pp 25–53
- Moseley ME, Feldman RA, Ortloff CR (1981) Living with crises: human perception of process and time. In: Nitecki M (ed) *Biotic crises in ecological and evolutionary time*. Academic, New York, pp 231–267
- Moy CM, Seltzer GO, Rodbell DT, Anderson DM (2002) Variability of El Niño/Southern Oscillation activity at millennial timescales during the Holocene epoch. *Nature* 420:162–165
- Muhs DR (1985) Age and paleo-climatic significance of Holocene sand dunes in Northeastern Colorado. *Association of American Geographers Annals* 75:566–682
- Muhs DR, Stafford TW Jr, Swinehart JB, Cowherd SD, Mahan SA, Bush CA, Madole RF, Maat PB (1997) Late Holocene eolian activity in the mineralogically mature Nebraska Sand Hills. *Quat Res* 48:162–176
- Mutai CC, Ward MN (2000) East African rainfall and tropical circulation/convection on intraseasonal to interannual timescales. *J Climate* 13:3915–3939
- Namias J (1970) Macroscale variations in sea surface temperatures in the North Pacific. *J Geophys Res* 75:565–582
- Nials FL, Deeds EE, Mosley ME, Pozorski SG, Feldman R (1979a) El Niño: the catastrophic flooding of coastal Peru. Part I *Field Mus Nat Hist Bull* 50(7):4–14
- Nials FL, Deeds EE, Mosley ME, Pozorski SG, Feldman R (1979b) El Niño: the catastrophic flooding of coastal Peru. Part II *Field Mus Nat Hist Bull* 50(8):4–10
- Nicholson S, Entekhabi D (1987) Rainfall variability in equatorial and Southern Africa: relationships with sea-surface temperature atmosphere coupling. *J Appl Meteorol Clim* 26:561–578
- Nicholson S, Kim J (1997) The relationship of the El Niño-Southern Oscillation to African rainfall. *Int J Climatol* 17:117–135
- Nigam S, Barlow M, Berbery EH (1999) Analysis links Pacific decadal variability to drought and streamflow in the United States. *EOS, Transactions, American Geophysical Union* 80:621–625
- Nunn PD (1994) *Oceanic islands*. Blackwell, Oxford, UK, p 418
- Nunn PD (2000) Environmental catastrophe in the Pacific Islands around A.D. 1300. *Geoarchaeology* 15:715–740
- Ogallal LJ, Janowiak JE, Halpert MS (1988). Teleconnections between East African seasonal rainfall and global sea surface temperature anomalies. *J Meteorol Soc Jpn* 66:807–822
- Otto-Bliessner BL, Brady EC, Shin SI, Liu Z, Shields C (2003) Modeling El Niño and its tropical teleconnections during the last glacial-interglacial cycle. *Geophys Res Lett* 30:2198 doi:10.1029/2003GL018553
- Petersen KL (1988) Climate and the Dolores River Anasazi: a paleoenvironmental reconstruction from a 10,000-year pollen record, La Plata Mountains, Southwestern Colorado. University of Utah Press, Salt Lake City
- Petersen KL (1994) A warm and wet Little Climatic Optimum and a cold and dry Little Ice Age in the Southern Rocky Mountains, U.S.A. *Clim Change* 26:243–269
- Peterson LC, Haug GH (2006) Variability in the mean latitude of the Atlantic Intertropical Convergence Zone as recorded by riverine input of sediments to the Cariaco Basin (Venezuela). *Palaeogeogr Palaeoclimatol Palaeoecol* 234(1):97–113
- Pfister C, Luterbacher J, Schwarz-Zanetti G, Wegmann M (1998) Winter air temperature variations in Western Europe during the Early and High Middle Ages (AD 750–1300). *Holocene* 8:535–552

- Poveda G, Mesa OJ (1996) Extreme phases of ENSO and their influence on the hydrology of Colombia. *Ing Hidrául Méx* XI:21–37
- Pozo-Vázquez D, Esteban-Parra MJ, Rodrigo FS, Castro-Diez Y (2001) The association between ENSO and winter atmospheric circulation and temperature in the North Atlantic region. *J Climate* 14:3408–3420
- Pozo-Vázquez D, Gamiz-Portis SR, Tovar-Pescador J, Esteban-Para MJ, Castro-Diez Y (2005) El Niño-Southern Oscillation events and associated winter European precipitation anomalies. *Int J Climatol* 25:17–31
- Proctor CJ, Baker A, Barnes WL, Gilmour MA (2000) A thousand year speleothem proxy record of North Atlantic climate from Scotland. *Clim Dyn* 16:815–820
- Proctor CJ, Baker A, Barnes WL (2002) A three thousand year record of North Atlantic climate. *Clim Dyn* 19:449–454
- Raab IM, Larson DO (1997) Medieval climatic anomaly and punctuated cultural evolution in coastal Southern California. *Am Antiq* 62:319–336
- Rajagopalan B, Cook E, Lall U, Rey BK (2000) Spatiotemporal variability of ENSO and SST teleconnections to summer drought over the United States during the 20th century. *J Clim* 13:4244–4255
- Rasmussen DM, Carpenter TH (1982) Variations in tropical sea surface temperature and surface wind fields associated with the Southern Oscillation/El Niño. *Mon Weather Rev* 110:354–384
- Redmond KT, Koch RW (1991) Surface climate and streamflow variability in the Western United States and their relationship to large-scale circulation indices. *Water Resour Res* 27:2381–2399
- Rein B, Lückge A, Sirocko F (2004) A major Holocene ENSO anomaly in the medieval period. *Geophys Res Lett* 31:L17211 doi:10.1029/2004GL020161
- Rein B, Lückge A, Reinhardt L, Sirocko F, Wolf A, Dullo W-C (2005) El Niño variability off Peru during the last 20,000 years. *Paleoceanography* 20 doi:10.1029/2004PA001099
- Rodbell DT, Seltzer GO, Anderson DM, Abbott MB, Enfield DB, Newman JH (1999) An ~15,000 year record of El Niño-driven alluviation in Southwestern Ecuador. *Science* 288:516–520
- Roeckner E, Bengtsson L, Feichter J, Lelieveld J, Rodhe H (1999) Transient climate change simulations with a coupled atmosphere-ocean GCM including the tropospheric sulphur cycle. *J Climate* 12:3004–3032
- Ropelewski CF, Halpert MS (1987) Global and regional scale precipitation patterns associated with the El Niño-Southern Oscillation. *Mon Weather Rev* 115:1606–1626
- Rowell DP, Ininda JM, Ward MN (1994) The impact of global sea surface temperature patterns on seasonal rainfall in East Africa. In: *Proc. Int. Conf. Monsoon Variability and Prediction*. Trieste, Italy, 9–13 May 1994, WMO/TD 619:666–672
- Schonher T, Nicholson SE (1989) The relationship between California rainfall and ENSO events. *J Clim* 2:1258–1269
- Seager R, Kushnir Y, Herweijer C, Naik N, Velez J (2005) Modeling of tropical forcing of persistent droughts and pluvials over Western North America: 1856–2000. *J Clim* 18:4065–4088
- Seimon A (2003) Improving climate signal representation in tropical ice cores. A case study from the Quelccaya Ice Cap, Peru. *Geophys Res Lett* 30:1772 doi:10.1029/2003GL017191
- Shabalova MV, van Engelen FV (2003) Evaluation of a reconstruction of winter and summer temperatures in the Low Countries. *Clim Change* 58:219–242
- Shimada I, Schaaf CB, Thompson LG, Mosley-Thompson E (1991) Cultural impacts of severe droughts in the prehistoric Andes: application of a 1,500-year ice core precipitation record. *World Archeology* 22:247–270
- Smith TM, Reynolds RW (2004) Extended reconstruction of global sea surface temperature data based on COADS data (1854–1997). *J Climate* 17:2466–2477
- Sridhar V, Loope DB, Swinehart JB, Mason JA, Oglesby RJ, Rowe CM (2006) Large wind shift on the Great Plains during the Medieval Warm Period. *Science* 313:345–347
- Starratt SW (2004) Diatoms as indicators of late Holocene freshwater flow variations in the San Francisco Bay estuary, Central California, USA. In: Poulin M (ed) *Proceedings of the Seventeenth International Diatom Symposium*, Ottawa, Canada, 25th–31st August 2002. Biopress, Bristol, UK, pp 371–397
- Stine SW (1990) Late Holocene fluctuations of Mono Lake, Eastern California. *Paleogeography, Paleoclimatology and Paleoecology* 78:333–381
- Stine S (1994) Extreme and persistent drought in California and Patagonia during medieval time. *Nature* 369:546–549
- Stott LD, Cannariato KG, Thunell R, Haug GH, Koutavas A, Lund S (2004) Decline of surface temperature and salinity in the western tropical Pacific Ocean in the Holocene epoch. *Nature* 431:56–59
- Swetnam TW (1993) Fire history and climate change in Giant Sequoia Groves. *Science* 262:885–889
- Thompson LG, Mosley-Thompson E, Arnao BM (1984) Major El Niño/Southern Oscillation events recorded in stratigraphy of the tropical Quelccaya Ice Cap. *Science* 226:50–52

- Thompson LG, Mosley-Thompson E, Henderson KA (2000) Ice-core palaeoclimate records in tropical South America since the last glacial maximum. *J Quat Sci* 15:377–394
- Timmermann A, Oberhuber J, Bacher A, Esch M, Latif M, Roeckner E (1999) Increased El Niño frequency in a climate model forced by future greenhouse warming. *Nature* 398:694–696
- Tourre YM, White WB (1995) ENSO signals in global upper-ocean temperature. *J Phys Oceanogr* 25:1317–1332
- van Engelen AFV, Buisman J, Jjnsen F (2001) A millennium of weather, winds and water in the Low Countries. In: Jones PD et al. (eds) *History and climate: memories of the future?* Kluwer Academic, New York, pp 101–124
- van Loon H, Madden RA (1981) The Southern Oscillation: Part I: Global associations with pressure and temperature in northern winter. *Mon Weather Rev* 109(109):1150–1672
- Verschuren D, Laird K, Cumming B (2000) Rainfall and drought in east Africa during the past 1100 years. *Nature* 403:410–414
- Vuille M, Bradley RS, Werner M, Healy R, Keimig F (2003a) Modeling $\delta^{18}\text{O}$ in precipitation over the tropical Americas: 1. Interannual variability and climatic controls. *J Geophys Res* 108(D6):4174 doi:10.1029/2001JD002038
- Vuille M, Bradley RS, Healy R, Werner M, Hardy DR, Thompson LG, Keimig F (2003b) Modeling $\delta^{18}\text{O}$ in precipitation over the tropical Americas: 2. Simulation of the stable isotope signal in Andean ice cores. *J Geophys Res* 108(D6):4175 doi:10.1029/2001JD002039
- Wallace JM, Gutzler DS (1981) Teleconnections in the geopotential height field during the Northern Hemisphere winter. *Mon Weather Rev* 109:784–812
- Wigand PE (1987) Diamond Pond, Harney County, Oregon: vegetation history and water table in the Eastern Oregon desert. *Great Basin Nat* 47:427–458
- Wigand PE (1997) A late Holocene pollen record from Lower Pahranaagat Lake, Southern Nevada, USA: high resolution paleoclimatic records and analysis of environmental responses to climate change. In: *Proceedings of the Thirteenth Annual Pacific Climate (PACLIM) Workshop*, Asilomar, CA, April 14–17, 1996. California Department of Water Resources Technical Report 53 of the Interagency Ecological Program for the Sacramento-San Joaquin Estuary, pp 63–77
- Wigand PE, Rhode D (2002) Great Basin vegetation history and aquatic systems: the last 150,000 years. In: Hershler R, Madsen DB, Currey DR (eds) *Great Basin aquatic systems history*. Smithsonian contributions to earth sciences 33. Smithsonian Institution, Washington, DC, pp 309–367
- Woodroffe CD, Gagan MK (2000) Coral microatolls from the Central Pacific record late Holocene El Niño. *Geophys Res Lett* 27:1511–1514
- Woodroffe CD, Beech MR, Gagan MK (2003) Mid-late Holocene El Niño variability in the equatorial Pacific from coral micro-atolls. *Geophys Res Lett* 30:1358 doi:10.1029/2002GL015868
- Yuan F, Linsley BK, Lund SP, McGeehin JP (2004) A 1200 year record of hydrologic variability in the Sierra Nevada from sediments in Walker Lake, Nevada. *Geochemistry, Geophysics and Geosystems* 5 2004 doi:10.1029/2003GC000652